HEALTH AND MEDICINE

Senolytic treatment for low back pain

Matthew Mannarino[1,2,3]†, Hosni Cherif[1,4]†, Saber Ghazizadeh[1], Oliver Wu Martinez[1], Kai Sheng[1,5], Elsa Cousineau[1], Seunghwan Lee[2,3,6], Magali Millecamps[2,3], Chan Gao[7], Alice Gilbert[3,8,9], Cedric Peirs[9], Reza Sharif Naeini[3,8], Jean A. Ouellet[1,4,5], Laura S. Stone[6,3], Lisbet Haglund[1,4,5]*

Senescent cells (SnCs) accumulate because of aging and external cellular stress throughout the body. They adopt a senescence-associated secretory phenotype (SASP) and release inflammatory and degenerative factors that actively contribute to age-related diseases, such as low back pain (LBP). The senolytics, *o*-vanillin and RG-7112, remove SnCs in human intervertebral discs (IVDs) and reduce SASP release, but it is unknown whether they can treat LBP. *sparc*$^{-/-}$ mice, with LBP, were treated orally with *o*-vanillin and RG-7112 as single or combination treatments. Treatment reduced LBP and SASP factor release and removed SnCs from the IVD and spinal cord. Treatment also lowered degeneration scores in the IVDs, improved vertebral bone quality, and reduced the expression of pain markers in the spinal cord. Together, our data suggest RG-7112 and *o*-vanillin as potential disease-modifying drugs for LBP and other painful disorders linked to cell senescence.

INTRODUCTION

Senescent cells (SnCs) accumulate in aging and degenerating tissues and are thought to directly contribute to disorders including heart disease, cancer (*1*–*3*), and osteoarthritis (*4*–*6*). Age-related accumulation is due to successive shortening of telomere length during replicative cycles (*7*, *8*). At the same time, stress-induced senescence can be induced prematurely by stressors such as DNA damaging agents, oxidative stress, mitochondrial dysfunction, load-induced injury, and disruption of epigenetic regulation (*9*, *10*). SnCs are resistant to apoptosis and, in addition to changes in their replicative status, release an array of factors collectively known as the *senescence-associated secretory phenotype* (*SASP*) (*1*). SASP factors encompass a diverse range of molecules such as pro-inflammatory, cytokines, chemokines, proteases, growth factors, catabolic enzymes, hemostatic factors, bioactive lipids, and reactive metabolites. The inflammatory environment triggered by SnCs prevents adjacent cells from maintaining tissue homeostasis (*11*, *12*) and induces senescence in a paracrine manner, thus exacerbating tissue deterioration (*13*). All SnCs share these general features, but there are distinct differences in SASP and antiapoptotic pathways linked to cell type, species, and senescence inducer (*14*, *15*).

Drugs that selectively target and remove SnCs (senolytic) have recently been identified (*16*, *17*). There are four main groups described to date targeting specific pro-senescence and antiapoptotic pathways: inhibitors of the Bcl-2 family of apoptosis regulatory proteins [D + Q (dasatinib + quercetin), ABT-199 (venetoclax), ABT-263 (navitoclax), and ABT-737]; inhibitors of the p53/MDM2 complex [UBX0101, RG7112, and USP7 inhibitors (P5091 and P22077)], which alleviate resistance to apoptosis; HSP-90 [17-DMAG (alvespimycin), 17-AAG (tanespimycin), geldanamycin, and ganetespib]; and phosphatidylinositol 3-kinase/Akt inhibitors (CUDC-907, FOXO4-DR, and PF-04691502) releasing proapoptotic transcription factors and natural flavonoids (fisetin, curcumin, quercetin, procyanidin C1, *o*-vanillin, apigenin, kaempferol, EF-24 (curcumin analog), genistein, and piperlongumine] with a less clear mode of action (*2*, *4*, *16*–*23*). Targeting indirectly related pro-senescence and antiapoptotic pathways has shown promising results with increased selectivity for SnCs in the absence of toxicity for normal proliferating or quiescent cells, as exemplified by the combination of dasatinib (D) and quercetin (Q) for age-dependent intervertebral disc (IVD) degeneration and age-related pathologies in mice (*24*–*28*).

Low back pain (LBP) is often related to IVD degeneration and is the number one global cause of years lived with disability (*29*–*32*). The personal costs of reduced quality of life and the economic cost to healthcare systems are enormous (*33*), exceeding $100 billion annually in the US alone (*34*). SnCs accumulate in degenerating IVDs and are proposed to directly contribute to disease progression and back pain (*5*, *35*–*44*). SASP factors, secreted by SnCs, generate a pro-inflammatory environment that accelerates the breakdown of the extracellular matrix (ECM) and worsens IVD degeneration (*24*, *43*, *45*, *46*). The protein $p16^{Ink4a}$ is a tumor suppressor and a marker of senescence that accumulates in the nucleus of SnCs, preventing cell cycle progression. Previous studies show that the deletion of $p16^{Ink4a}$ in mice prevents the accumulation of SnCs, reduces SASP, and mitigates age-related IVD degeneration (*36*, *47*, *48*). Together, these studies indicate that senolytic drugs may reduce SASP-driven damage and potentially slow or reverse the degenerative processes. The senolytic drugs *o*-vanillin and RG-7112 remove human senescent IVD cells and reduce SASP factor release from cells and intact IVDs (*49*–*52*). The senolytic drug RG-7112 is a p53/MDM2 complex inhibitor. *o*-Vanillin is a natural senolytic and senomorphic substance that has been shown to reduce senescence burden and SASP factor release and to improve tissue homeostasis in human IVDs (*49*, *50*, *53*), indicating that they could potentially reduce pain.

The primary manifestation of IVD morbidity in humans is LBP, which cannot be evaluated in cell and tissue culture experiments. Here, we turned to the *sparc*$^{-/-}$ mouse model to determine whether RG-7112 and *o*-vanillin can attenuate behavioral indices of pain and IVD degeneration without causing adverse effects. SPARC (secreted

[1]Department of Surgery, Orthopaedic Research Lab, McGill University, Montreal, QC, Canada. [2]ABC-platform (Animal Behavioral Characterization) at the Alan Edwards Centre for Research on Pain, McGill University, Montreal, QC, Canada. [3]Alan Edwards Centre for Research on Pain (AECRP), McGill University, Montreal, QC, Canada. [4]Department of Surgery, McGill Scoliosis and Spine Group, McGill University, Montreal, QC, Canada. [5]Shriner's Hospital for Children, Montreal, QC, Canada. [6]Department of Anesthesiology, University of Minnesota, Minneapolis, MN, USA. [7]Division of Physiatry, Department of Medicine, McGill University, Montreal, QC, Canada. [8]Department of Physiology and Cell Information Systems, McGill University, Montreal, QC, Canada. [9]Université Clermont-Auvergne, CHU Clermont-Ferrand, Inserm, Neuro-Dol, Clermont-Ferrand, France.
*Corresponding author. Email: lisbet.haglund@mcgill.ca
†These authors contributed equally to this work.

protein acidic and rich in cysteine) is one of the most down-regulated genes in IVDs of patients with LBP. The SPARC protein is highly expressed in nondegenerate human IVDs, while individuals with IVD degeneration have reduced levels correlated with ECM breakdown, collagen deterioration, and increased inflammatory environment. In accordance, mice lacking the *sparc* gene develop early-onset IVD degeneration that is well established by 7 months of age (*54*–*65*). The primary objective of this study was to determine whether *o*-vanillin and RG-7112 remove SnCs, reduce inflammatory mediators, and relieve pain in middle-aged *sparc*$^{-/-}$ mice with established IVD degeneration and back pain. The secondary objective was to evaluate whether a combination of the drugs provides a better effect than either drug alone.

RESULTS

Validation of the *sparc*$^{-/-}$ mice model to study senescence

SnCs are suggested to contribute to IVD-related LBP in human patients, and removing them in human IVD tissue and cell cultures decreases the expression of inflammatory and pain-mediating SASP factors. Human patients with IVD degeneration and LBP have epigenetic modifications and reduced sparc gene and protein expression in degenerating IVDs (*61*, *66*). Similarly, animals with the *sparc* gene deleted develop age-related LBP that is well established by 7 months of age. Like in human patients, IVDs in the lower lumbar spine are more affected than higher lumbar levels. In addition, *sparc*$^{-/-}$ mice present with a higher degree of degeneration than *wt* mice, with the greatest difference in the lower lumbar spine at 7 and 9 months of age (Fig. 1, A and B, and fig. S1, A and B). We found that *sparc*$^{-/-}$ mice, like humans, accumulate SnCs in their IVDs with age and degeneration. In the lower lumbar spine (L3-S1), the nucleus pulposus (NP) region had a threefold and the annulus fibrosis (AF) region a sixfold higher level of *p16*^{Ink4a}-positive SnCs when comparing age-matched *sparc*$^{-/-}$ and wild-type animals. The upper levels (T13-L3) show significantly less degeneration and fewer SnCs, although, compared to the wild type, there is a slight but statistically significant increase in degeneration and *p16*^{Ink4a}-positive SnCs in both the NP and AF at 9 months of age (Fig. 1, C and D, and fig. S1C). An increase in the level of SnCs and the degree of IVD degeneration was strongly correlated [coefficient of determination (R^2) = 0.85] (Fig. 1E).

Next, we performed bulk RNA sequencing (RNA-seq) to evaluate whether senescence-associated genes were enriched in IVDs of *sparc*$^{-/-}$ mice. Although the difference in degenerative changes and the level of senescence is less pronounced in the upper levels (T13-L3), these were used to minimize the number of animals used in the study. Spearman correlation was computed to examine the variance and the relationship of global gene expression across the samples. Principal components analysis (PCA) shows a clear separation between wild-type and *sparc*$^{-/-}$ mice (Fig. 1F). We identified 489 differentially expressed genes, 194 significantly up-regulated and 295 significantly down-regulated in *sparc*$^{-/-}$ mice (Fig. 1G). A significant enrichment was detected in genes regulating senescence [*cdk2a*, *cdk2ai*(*p16*^{Ink4a}), *E2F7*, *EIF4*, *CDC25a*, *CDC42*, *cdk2d*, *cdk12*, and *TNFRSF1b*] and SASP factors (*IL1b*, *IL1R2*, *CCL6*, *CCR6*, ADAM8, *TLR-1*, *TLR-2*, *TLR-7*, and *TLR-9*) (Fig. 1H). Gene set enrichment analysis (GSEA) comparing our data to those presented by the Human Molecular Signatures Database (MSigDB), Reactome, and SenMayo revealed an up-regulation of pathways involved in senescence [normalized enrichment score (NES) = 1.52 and 1.02], G_2-M cell cycle checkpoints (NES = 2.62), and SASP factors release (NES = 1.92) in *sparc*$^{-/-}$ animals (Fig. 1I). The complete list of genes, together with the list of enriched genes and the enrichment scores of each dataset, can be found in tables S1 to S6.

A multiplex assay was used to investigate the level of inflammatory mediators systemically in *sparc*$^{-/-}$ and wild-type animals. The blood concentration of CXCL-1, CXCL-5, CXCL-9, CXCL-10, interleukin-1β (IL-1β), IL-6, tumor necrosis factor–α (TNF-α), CCL-2, CCL-7, and vascular endothelial growth factor–α (VEGF-α) showed no significant difference between *sparc*$^{-/-}$ and wild-type animals (Fig. 1, J to S).

To evaluate the influence of senescence and SASP in the IVDs, a multiplex assay was used to measure the release of 15 SASP factors from lumbar discs (L4-S1) where degeneration and senescence are prominent in *sparc*$^{-/-}$ animals. Ten of the 15 SASP factors (CXCL-1, CXCL-5, CXCL-9, CXCL-10, IL-1β, IL-6, TNF-α, CCL-2, CCL-7, and VEGF-α) assessed showed significantly higher release in *sparc*$^{-/-}$ compared to that in wild-type IVDs. Three factors [IL-2, IL-10, and macrophage colony-stimulating factor (M-CSF)] did not show a difference, and two factors [interferon-γ (IFN-γ) and receptor activator of nuclear factor-κB ligand (RANKL)] were undetected (fig. S2, A to M, and table S7). Together, this information provides the rationale for evaluating senotherapeutics as a potential treatment for LBP in this model.

The phenotype of SnCs is heterogeneous and can differ between species. Therefore, isolated IVDs were treated in culture before treating live animals to evaluate whether *o*-vanillin and RG-7112 can also target SnCs and reduce SASP factors in mice. The selected drug concentrations were based on previous studies with human IVD cells and intact human IVDs (*49*–*52*). The same 10 factors elevated in *sparc*$^{-/-}$ IVDs were all reduced, with 9 of 10 significantly reduced, following ex vivo treatment with either *o*-vanillin or RG-7112. All 10 factors were further reduced with a combination of the drugs at the highest concentration (fig. S2, A to M, and table S7). These data demonstrate that *o*-vanillin and RG-7112 are efficacious in mouse IVDs and could potentially affect IVD degeneration and back pain if they reach the target tissues. Because it is not possible to evaluate whether treatment can reduce perceived pain in ex vivo studies, our next step was to evaluate whether treatment can reduce perceived pain.

Senotherapeutics reduced pain in *sparc*$^{-/-}$ mice

Sparc$^{-/-}$ mice start showing signs of LBP at 4 months of age and have well-established pain by 7 months (*54*–*56*). We compared male and female *sparc*$^{-/-}$ and wild-type animals over 8 weeks (7 to 9 months of age) as a baseline for pain behavior. Grip strength and tail suspension were used to determine axial pain, while von Frey and acetone-evoked behavior were used to evaluate radiating pain (*54*–*56*, *60*, *67*). The experimental design and treatments are depicted in Fig. 2A. As expected, *sparc*$^{-/-}$ animals showed well-established behavioral signs of LBP that progressively worsened over the 8-week period, whereas wild-type animals showed consistent no-pain phenotype (Fig. 2, B to I). *sparc*$^{-/-}$ animals were treated weekly by oral gavage to establish whether oral treatment with *o*-vanillin and RG-7112 reduced LBP. The concentrations were extrapolated from the ex vivo studies by converting the highest optimal concentration in culture (in micromolar) to the highest dose in vivo (in milligrams per kilogram) (*68*–*70*) as outlined in Table 1. Pharmacokinetic (PK) parameters

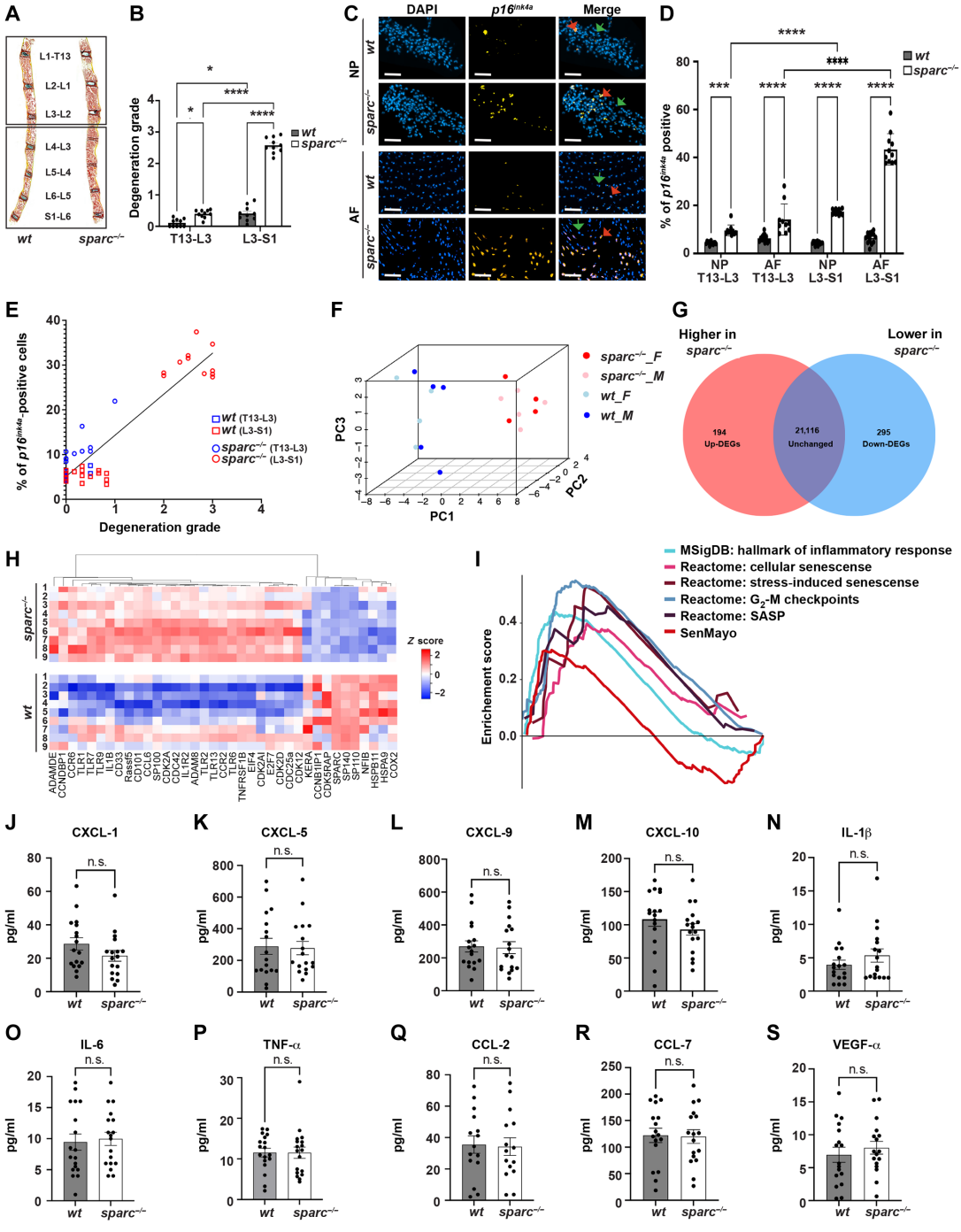

Fig. 1. Validation of senescence in 9-month-old *sparc*$^{-/-}$ IVDs. (**A**) Representative images of multichromatic FAST (Fast Green, Alcian Blue, Safranin-O, and tartrazine)–stained sections *sparc*$^{-/-}$ and wild-type spines. (**B**) Quantification of the histological degeneration grade in the upper (T13-L3) and lower (L3-S1) lumbar IVDs ($n = 10$ animals per strain). (**C**) Photomicrographs showing *p16*^{Ink4a}-positive nucleus pulposus (NP) and annulus fibrosis (AF) cells with 4′,6-diamidino-2-phenylindole (DAPI) counterstain. The red arrows point to *p16*^{Ink4a}-positive cells, and the green arrows indicate non-SnCs. (**D**) Quantifying of *p16*^{Ink4a}-positive IVD cells. (**E**) Scatter plot showing the correlation between IVD degeneration and *p16*^{Ink4a}-positive cells ($n = 6$ to 8 WT and 9 *sparc*$^{-/-}$ animals per strain). (**F**) Principal components analysis (PCA) analysis showing the transcriptomic signatures in upper IVDs. (**G**) Venn diagram of differentially expressed genes (DEGs). PC, principal component. (**H**) Heatmap showing the expression of 37 senescence and SASP-associated genes. Data shown are relative to the calculated *z* scores across the samples and ranked by significance adjusted to $P < 0.05$. Red represents relatively high expression, and blue represents relatively low expression ($n = 9$ animals per strain). (**I**) Multiplex gene set enrichment analysis (GSEA) of the SenMayo, Reactome (cellular senescence, SASP, stress-induced senescence, and G_2-M checkpoints), and inflammatory response (MSigDB) gene sets upper (T13-L3) IVDs. Nominal *P* value, calculated as a two-sided *t* test, with no adjustment since only one gene set was tested ($n = 9$ animals per strain). (**J** to **S**) Luminex evaluation of circulating SASP factors ($n = 18$ animals per strain). Values are presented as means ± SD; significance was evaluated by a two-tailed unpaired *t* test in (B) and repeated-measures one-way analysis of variance (ANOVA) in (D) and (J) to (S). Significance is indicated as $^*P < 0.05$, $^{***}P < 0.001$, and $^{****}P < 0.0001$. n.s., not significant.

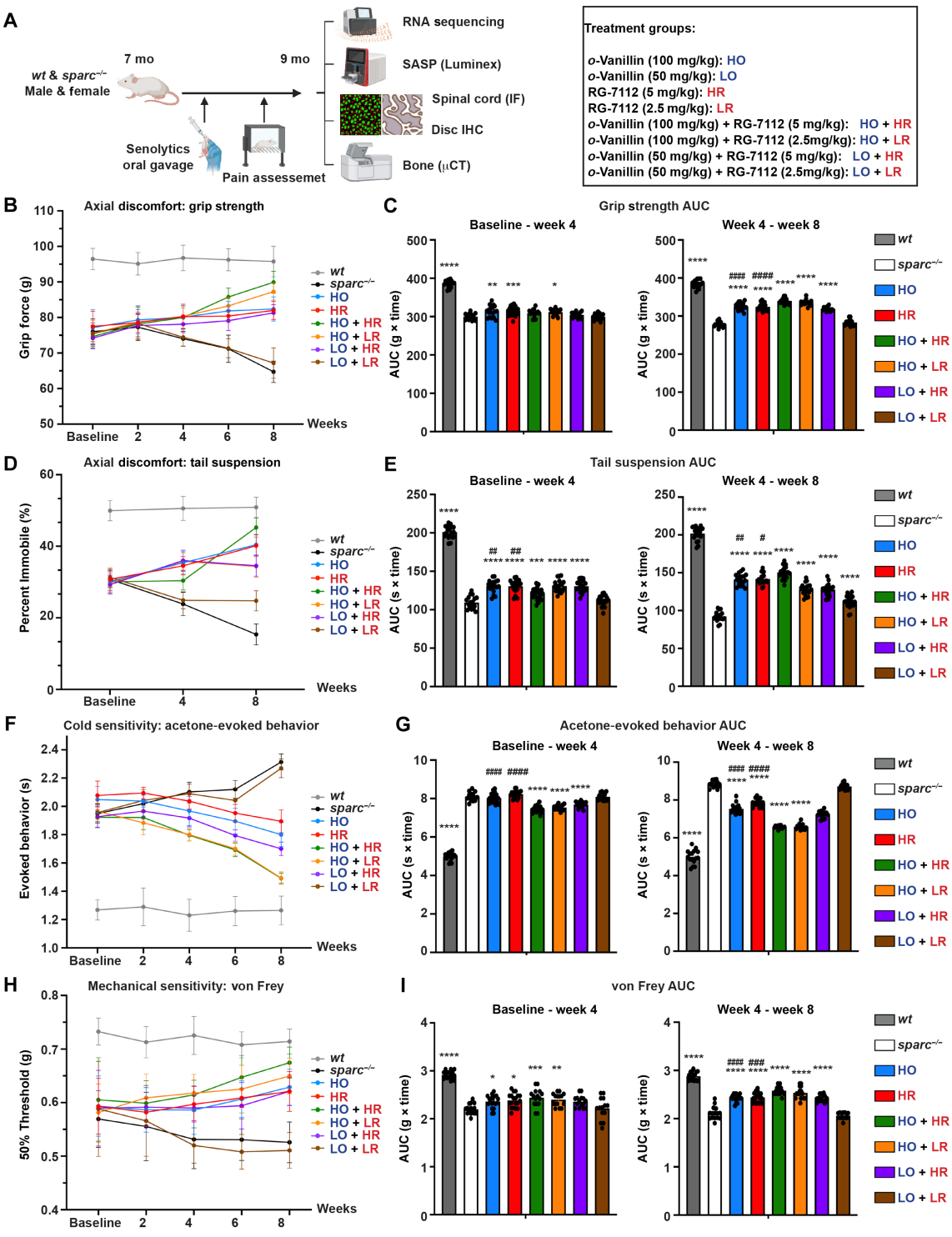

Fig. 2. Targeting SnCs with senolytic drugs improves axial discomfort, cold, and mechanical sensitivity in *sparc*$^{-/-}$ mice. (**A**) Schematic of the experimental setup. Animals received vehicle or senolytic treatment weekly through oral gavage [as described in the treatment groups (box)]. Pain assessment tests were performed every 2 weeks (grip strength, acetone-evoked behavior, and von Frey) and every 4 weeks for tail suspension. mo, months; μCT, micro–computed tomography; IF, immunofluorescence; IHC, immunohistochemistry. Axial pain was assessed by (**B**) grip strength and (**D**) tail suspension tests. Radiating pain was assessed by (**F**) acetone-evoked behavior (cold sensitivity) and (**H**) von Frey (mechanical sensitivity) tests. The area under the curve (AUC) between baseline and week 4 and between week 4 and week 8 was calculated using the trapezoid method $[(T2 - T1) \times (B1 + B2)/2]$, where T is time and B is the behavioral score for (**C**) grip strength, (**E**) tail suspension, (**G**) acetone-evoked behavior, and (**I**) von Frey assay. $n = 14$ to 20 animals per group (7 to 10 males and 7 to 10 females). Data are presented as means ± SEM and analyzed by one-way ANOVA followed by Tukey's post hoc test (C, E, G, and I). */#$P < 0.05$, **/##$P < 0.01$, ***/###$P < 0.001$, and ****/#### $P < 0.0001$. * indicates a significant difference compared with *sparc*$^{-/-}$, and # indicates a significant difference compared with single-drug treatment.

Table 1. Concentration and annotation for each of the treatment groups.

Senotherapeutics	Annotation	Concentration (mg/kg)
o-Vanillin	HO	100 mg/kg
o-Vanillin	LO	50 mg/kg
RG-7112	HR	5 mg/kg
RG-7112	LR	2.5 mg/kg
o-Vanillin + RG-7112	HO + HR	100 mg/kg + 5 mg/kg
o-Vanillin + RG-7112	HO + LR	100 mg/kg + 2.5 mg/kg
o-Vanillin + RG-7112	LO + HR	50 mg/kg + 5 mg/kg
o-Vanillin + RG-7112	LO + LR	50 mg/kg + 2.5 mg/kg

and bioavailability of both drugs are presented in fig. S3 (A and B) and tables S10 to S16. Both drugs improved the pain phenotype and significantly improved axial discomfort (grip strength and tail suspension), cold sensitivity (acetone-evoked behavior), and radiating pain (von Frey) after 4 weeks of treatment, with all assessments significantly improving after 8 weeks of treatment (Fig. 2, B to I). To determine whether the drugs provide synergistic or additive effects, they were combined at 100 + 100% (HO + HR), 100 + 50% (HO + LR), 50 + 100% (LO + HR), or 50 + 50% (LO + LR) of the single-drug concentrations. After 8 weeks of treatment, combining the drugs with at least one at the high dose significantly enhanced the effect. The attenuation of pain behavior was lost in all tests except tail suspension when both drugs were given at the low dose (50%) (Fig. 2, B to I).

Male and female animals are shown together as no significant sex differences were found. We found no difference in the weight, mortality, body weight, or distance traveled (open-field assay) between the groups (fig. S4, A to D). The data demonstrate that both drugs can reduce behavioral indices of back pain and that combining them within the higher concentration range further reduces pain.

Senotherapeutics reduced SASP factor release

As shown above, IVDs from *sparc*$^{-/-}$ animals release measurable and elevated levels of SASP factors that could contribute to LBP (fig. S2, A to M). To determine whether the oral treatment reduced SASP factor release, a set of lumbar IVDs was harvested at the termination of the 8-week treatment, and the release of the same 15 SASP factors was measured. Both drugs significantly reduced the release of 10 factors (CXCL-1, CXCL-5, CXCL-9, CXCL-10, CCL-2, CCL-7, IL-1β, IL-6, TNF-α, and VEGF-α). The combination treatment provided an additive effect and further significantly reduced the release of the same 10 factors. Although significantly lower than untreated, reducing either drug by 50% of the single-drug concentrations did not provide any added effect, and reducing both to 50% was less effective than the single drugs at 100% (Fig. 3, A to L). Two factors, IL-2, and IL-10, were only significantly decreased by *o*-vanillin, while M-CSF was significantly decreased by RG-7112 when single drugs were applied. A significant additive effect was observed for IL-10 and M-CSF following combination treatment (Fig. 3, H, G, and M). The measured concentrations and significance are shown in table S8.

Senotherapeutics reduced senescent IVD cells and improved disc degeneration score

Next, we evaluated whether the number of *p16*^{Ink4a}-positive SnCs was reduced in the IVDs and whether treatment could improve IVD health. Single-drug treatment significantly reduced the number of *p16*^{Ink4a}-positive cells (~40%) from both the NP and AF regions (Fig. 4, A and B). Combination treatment provided a further significant (25 to 27%) reduction in both regions when at least one of the drugs was kept at 100%; reducing both by 50% did not provide an additive effect (Fig. 4, A and B). Previous treatment modalities have shown pain reduction in the *sparc*$^{-/-}$ model, but no drugs to date have been able to improve histological degeneration score (*54*–*56*, *60*, *65*, *67*, *71*, *72*). We show that both drugs improved histological degeneration score (Fig. 4, C and D). Combining the drugs at 100% provided a significant additive effect, while lowering one to 50% remained at the level of single drugs and lowering both by 50% failed to improve histological degeneration grade (Fig. 4E).

Senotherapeutics decreased SnCs and pain mediators in the spinal cord

SnCs have also been detected in various cell types in the central nervous system (CNS), including neural and glial cells, where their presence could contribute to a pain phenotype (*73*–*77*). We found a 4.8-fold significantly larger area of *p16*^{Ink4a} immunoreactivity in the dorsal horn of *sparc*$^{-/-}$ mice compared to that of wild type (Fig. 5, A and B). Using confocal microscopy, we also confirmed the *p16*^{Ink4a} immunoreactivity colocalized with nuclear 4′,6-diamidino-2-phenylindole (DAPI) staining (fig. S5A). Systemic senotherapeutic treatment could directly affect pain signaling in the spinal cord and contribute to the reduction of pain. We found a significant reduction of 24 to 30% in *p16*^{Ink4a} reactivity with single drugs compared to untreated *sparc*$^{-/-}$; combining them further significantly reduced the *p16*^{Ink4a} immunoreactivity by 64% compared to untreated *sparc*$^{-/-}$. The effect was lost when both senolytics were reduced by 50% (Fig. 5C). As previously reported, *sparc*$^{-/-}$ mice have increased immunoreactivity for calcitonin gene-related peptide (CGRP), glial fibrillary acidic protein (GFAP), and the activated microglia marker protein (cd11-b) in the dorsal horn of the spinal cord that may contribute to the pain phenotype (Fig. 5D and fig. S5B) (*58*, *60*, *67*). The immunoreactivity of CGRP was significantly reduced in mice treated with single drugs (52 to 55%). Combining them further significantly reduced CGRP immunoreactivity (~60%) with a lower (20%) but significant effect observed even when both were reduced by 50% (Fig. 5E). Activated microglia and astrocytes in the dorsal horn of the spinal cord are known to contribute to the development of chronic pain (*78*). GFAP immunoreactivity was reduced by single-drug treatment (42 to 44%) with combination treatment keeping the higher *o*-vanillin concentration, further reducing GFAP immunoreactivity (7 to 13%) (Fig. 5F). Lowering *o*-vanillin in the combination

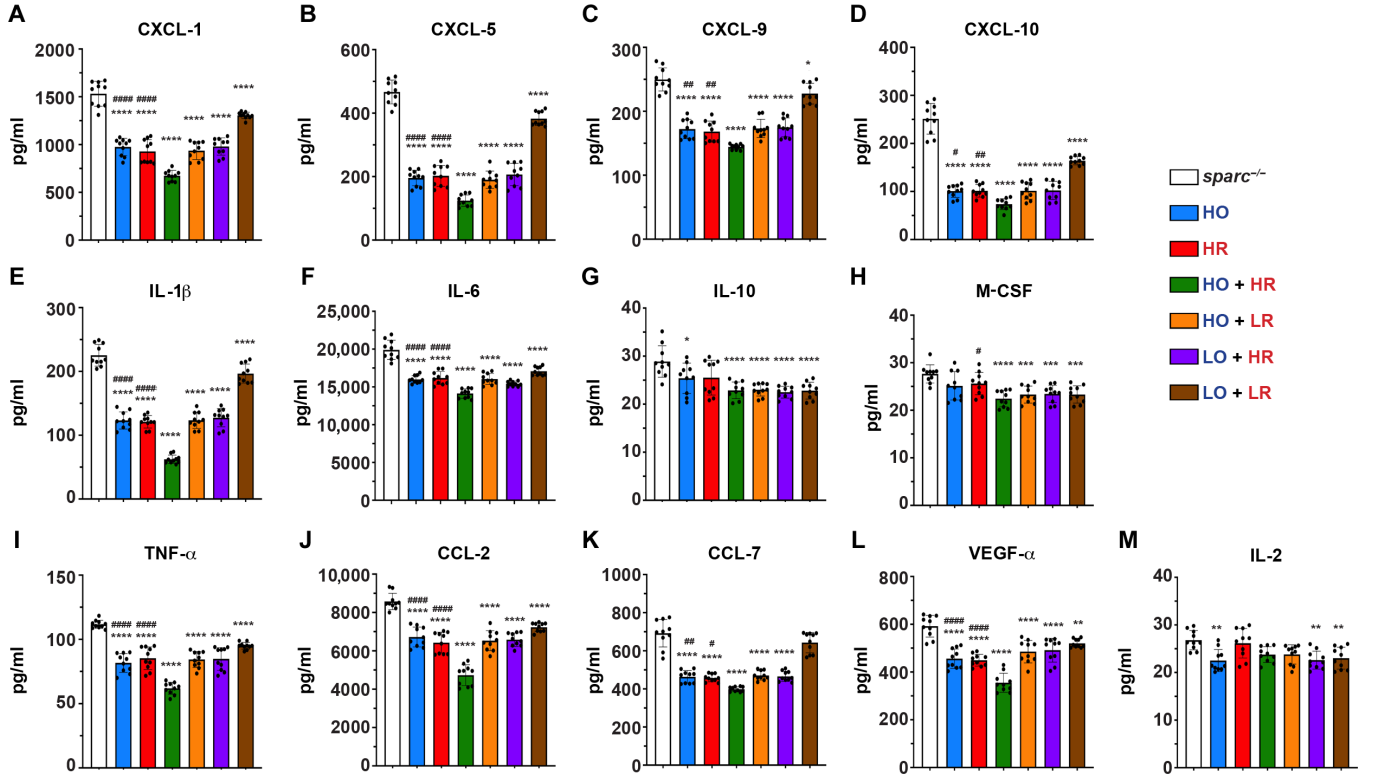

Fig. 3. SASP factor release is reduced in treated 9-month-old *sparc*$^{-/-}$ mice. IVDs (L3-S1) from *sparc*$^{-/-}$ mice treated with senolytics or vehicle were isolated, and the release of 15 SASP factors was evaluated. The release of chemokines (**A** to **D**, **J**, and **K**), cytokines (**E** to **G**, **I**, and **M**), and growth factors (**H** and **L**) was assessed using a multiplex assay. The data in (A) to (M) are presented as means ± SD; two-way ANOVA and post hoc comparison Tukey's were used to measure significant differences between the groups. */#$P < 0.05$, **/##$P < 0.01$, ***$P < 0.001$, and ****/####$P < 0.0001$. * indicates a significant difference compared with *sparc*$^{-/-}$, and # indicates a significant difference compared with single-drug treatment. Four discs represent one measure per animal. $n = 10$ animals (5 males and 5 females) in each group.

treatments did not provide an added effect over single drugs. CD11-b immunoreactivity was also significantly reduced with single drugs (40 to 42%); the effect was further reduced (62%) with the combination treatment at the highest concentration. Lowering one did not provide an additive effect over single drugs, and an effect was lost when both were given at 50% (Fig. 5G). These results suggest that senotherapeutics could be contributing to reducing back pain by decreasing pain-related neuroplasticity and glial cell activity.

Senotherapeutics increased disc volume and improved bone parameters

In addition to IVD degeneration and LBP, *sparc*$^{-/-}$ mice are known to have osteopenia that is also a potential contributor to LBP. Recent studies have demonstrated that senolytic drugs can improve age-related bone loss. We, therefore, treated a second cohort of animals to evaluate whether oral administration of *o*-vanillin and RG-7112 could improve bone quality in *sparc*$^{-/-}$ mice. We treated *sparc*$^{-/-}$ animals with single and combination treatments, keeping the drug concentrations at the higher levels (HO, HR, and HO + HR). Micro–computed tomography (CT) analysis was performed, and we evaluated IVD volume and vertebral bone quality. Previous studies have shown a reduced disc height index in *sparc*$^{-/-}$compared to that in wild-type mice and our analysis demonstrated a significantly lower IVD volume (~34%) in the 9-month-old *sparc*$^{-/-}$ group (Fig. 6, A and B). Treatment with the two drugs as single treatments showed a trend toward improvement in disc volume compared to that in vehicle-treated mice. In contrast, a significant increase (~27%) in disc volume was found following combination treatment with the drugs at the high dose (Fig. 6C; fig. S4, A and B; and movies S1 to S5). Three-dimensional (3D) reconstructions representing vertebrae of treated and untreated animals are illustrated in Fig. 6D, fig. S4 (A and B), and movies S1 to S5. Analysis of bone microarchitecture was performed in a region starting just above the growth plate to the beginning of the pedicels as illustrated in (fig. S4B). The trabecular microarchitecture revealed a significantly lower bone density (56%), trabecular thickness (Tb. Th; 15%), and trabecular number (Tb. N; 50%) in 9-month-old *sparc*$^{-/-}$ compared to those in wild-type mice (Fig. 6, G and I). In contrast, trabecular separation (Tb. Sp) was significantly higher (42%) in *sparc*$^{-/-}$compared to that in wild-type mice (fig. S4C). Single treatment of *sparc*$^{-/-}$ animals resulted in a significantly increased bone density, bone volume fraction (BV/TV) (52 and 69%) that was somewhat stronger (85%) and more significant in response to the combination treatment (Fig. 6J). Similarly, each drug alone or as combination treatment resulted in a significant increase in Tb. N (34.1, 48, and 47%) (Fig. 6K). Tb. Th was significantly increased only following treatment with RG-7112 and combination (15 and 23%) (Fig. 6L). No significant improvement was observed in Tb. Sp for any of the treatment groups (fig. S4D).

Cortical bone parameters measured in the region of interest (ROI) described in fig. S4B showed a significantly lower bone volume (BV; 45%), moment of inertia (MMI; 72%) (Fig. 6, M and N),

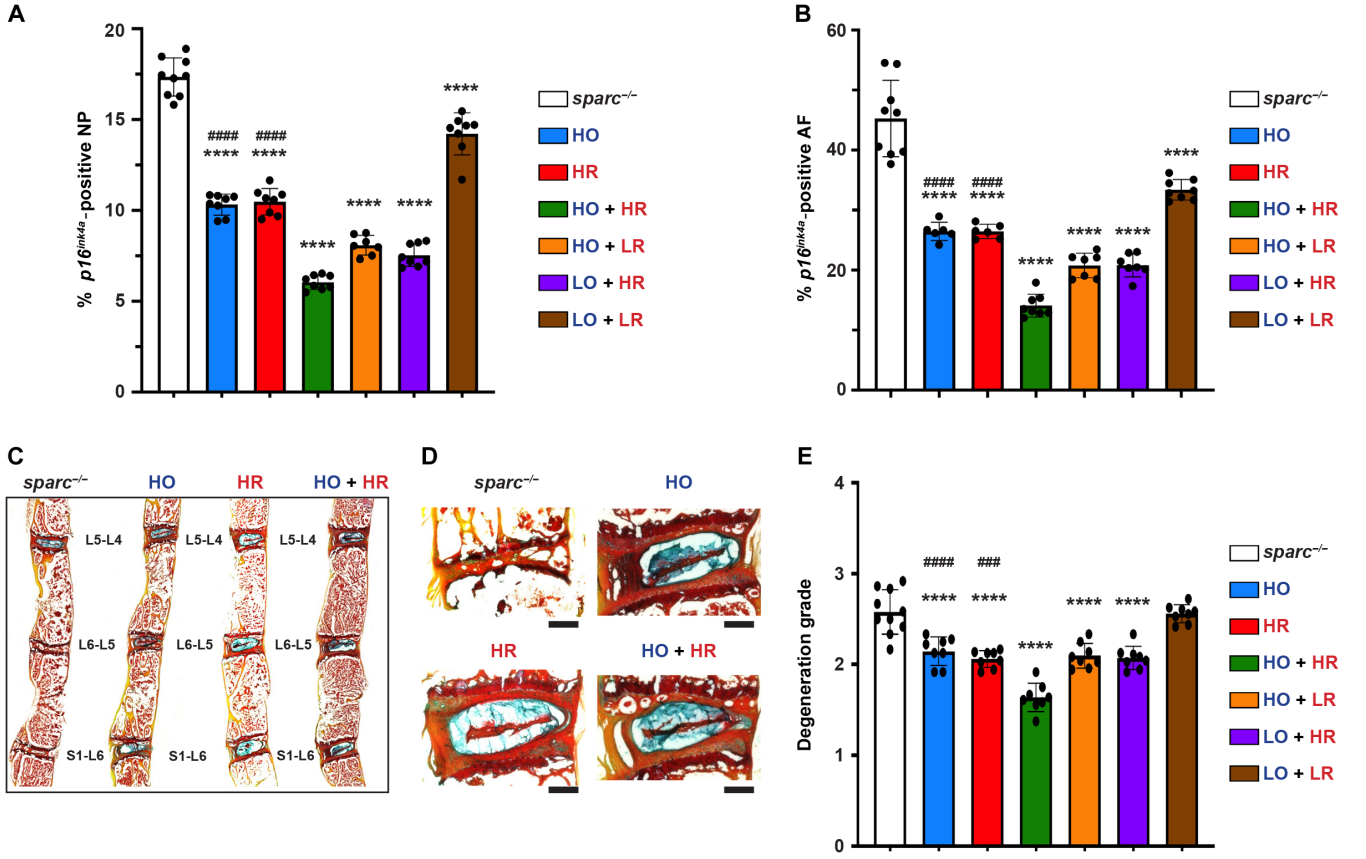

Fig. 4. Senolytics removed SnCs and improved IVD health. *sparc*$^{-/-}$spines (L3-S1) from animals treated with senolytics or vehicle (n = 7 to 9 animals, 3 to 5 males and 4 to 5 females per group) were collected and processed for histological evaluation. Immunofluorescence staining measures the percentage of *p16*^{Ink4a}-positive cells; DAPI was used as a counterstain (**A**) NP and (**B**) AF. (**C**) Representative images of lumbar IVDs (L3-S1) from *sparc*$^{-/-}$ mice treated with senolytics or vehicle. (**D**) FAST staining revealed histological improvement in the ventral region (clear distinction between AF and NP and increase in disc height) of treated discs. (**E**) Histological degeneration grade of the IVDs was independently evaluated and the average grade per animal is presented for a total of 8 to 10 animals (4 to 5 males and females) per group. Statistical comparisons were calculated using an ordinary two-way ANOVA, with a Tukey's post hoc analysis. Data are presented as means ± SD. ###P < 0.001 and ****/####P < 0.0001. * indicates a significant difference compared with *sparc*$^{-/-}$, and # indicates a significant difference compared with single-drug treatment.

and cross-sectional thickness (Cs. Th; 8%) (fig. S6E) in 9-month-old *sparc*$^{-/-}$ compared with those in wild-type mice. Both single and combination treatments significantly increased the BV (48, 67, and 63%), the increase in MMI although significant was more variable with no further improvement with the combination treatment (Fig. 6, O and P). Cs. Th measures revealed no significant difference between any of the groups (fig. S6F). [The values for disc and bone parameters are detailed in table S9 and baseline parameters in 7-month-old animals in fig. S1 (E to K).] In summary, our findings suggest that oral administration of senolytics improves IVD and bone health with a more robust improvement when *o*-vanillin and RG-7112 are administered as a combination treatment.

DISCUSSION

Reducing the burden of SnCs or selectively killing them with senomorphic or senolytic drugs holds great promise for the treatment or prevention of musculoskeletal-related diseases (*79*). An elevated level of SnCs is found in degenerating human IVDs (*35*, *36*, *48*, *80*), where recent studies suggest them as a hallmark and major cause of back pain and IVD degeneration (*40*, *42*, *47*, *81*). Clearance of SnCs has been shown to delay age-related changes in mice, and, as IVD degeneration and LBP are closely linked, senolytic drugs could potentially be a promising therapy for the disease (*24*, *43*, *44*, *48*). In this study, we show that oral treatment with RG-7112 and *o*-vanillin reduced behavioral indices of LBP, reduced SASP factor release from the IVDs, and removed SnCs from the IVD and spinal cord. We also found that treatment lowered the degeneration score of the IVD, reduced the expression of pain markers in the dorsal horn of the spinal cord, and improved vertebral bone quality. Together, our findings suggest that treatment with RG-7112 and *o*-vanillin can reduce LBP and improve tissue health, with the most prominent effect when applied in combination.

We previously described the two compounds, the natural compound *o*-vanillin and synthetic drug RG-7112, have senolytic effects on senescent IVD cells. Both senolytics reduce the release of SASP factors in isolated IVD cells and intact human IVDs (*49*, *50*). SnCs are heterogeneous, and recent reports suggest that a combination of drugs targeting multiple pathways could improve treatment outcomes (*79*, *82*, *83*). *o*-Vanillin and RG-7112 target distinct senescence-associated networks, and we found that combining them greatly enhanced the senotherapeutic effect on senescent human IVD cells (*52*).

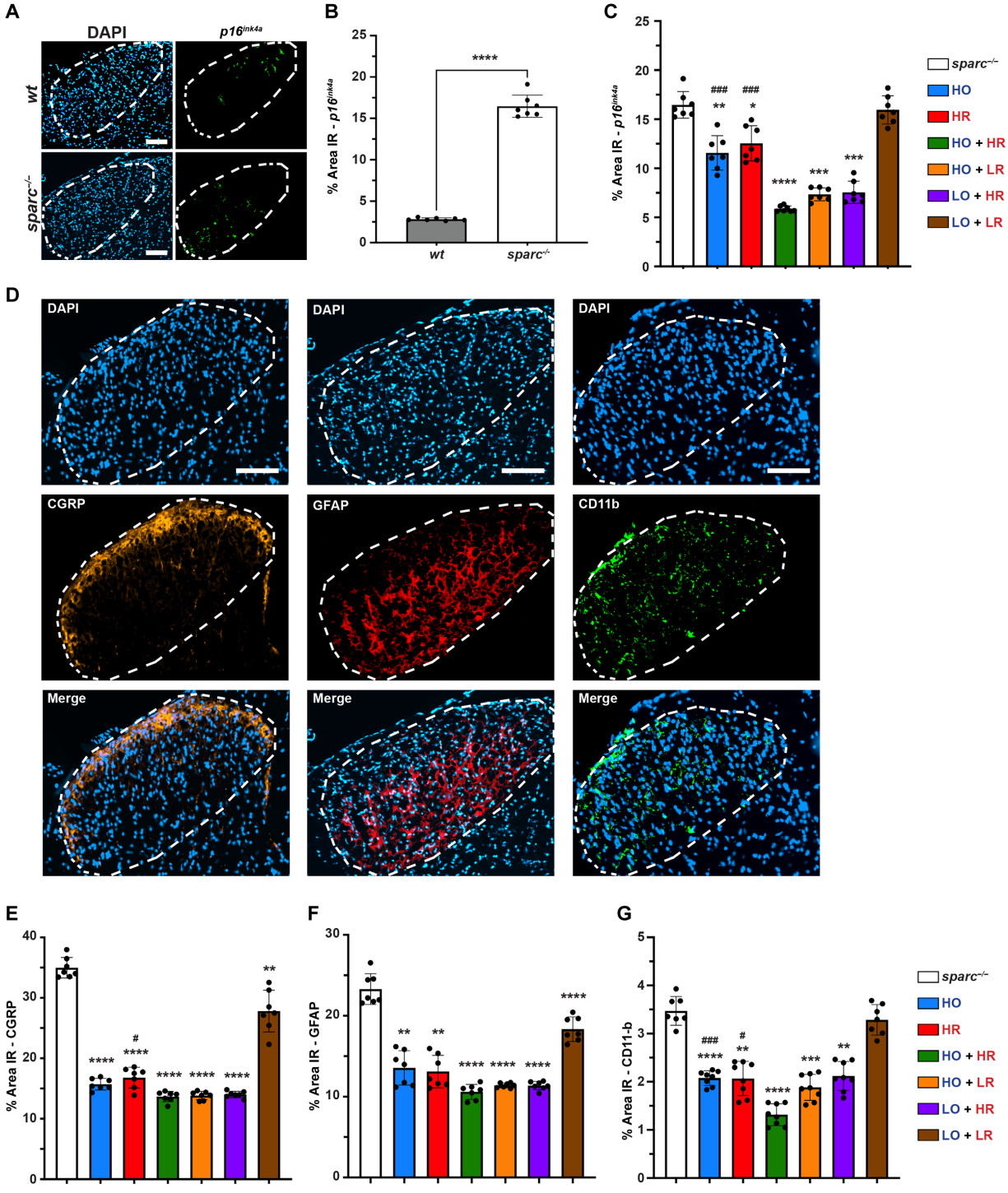

Fig. 5. Senolytics reduced SnCs and pain-related neuroplastic changes in the spinal cord of *sparc*$^{-/-}$ mice. (**A**) Spinal cords from perfused animals treated with senolytic drugs or vehicle were collected and processed for histological evaluation. Representative images showing higher *p16*^{Ink4a} immunoreactivity in the dorsal horn (delineated in dashed line) in *sparc*$^{-/-}$ compared to that in wild-type mice at 9 months. (**B**) Quantification of the increased immunoreactivity (percentage area) (% Area IR). (**C**) *p16*^{Ink4a} immunoreactivity was reduced in treated *sparc*$^{-/-}$ animals. The spinal cords were also assessed for pain-related neuroplastic changes. (**D**) Representative images of calcitonin gene-related peptide (CGRP), glial fibrillary acidic protein (GFAP), and CD11b immunoreactivity in the dorsal horn of *sparc*$^{-/-}$ mice (delineated in a dashed line). The immunoreactivity (percentage area) was quantified for (**E**) CGRP, (**F**) GFAP, and (**G**) CD11b. The % area with immunoreactivity above a set threshold was calculated from the total area of the dorsal horn. $n = 7$ to 8 animals per group (3 to 4 males and 4 females). DAPI was used as a counterstain. The average of three separate images was calculated for each animal and used to calculate the mean of the treatment group. Scale bars (A and D), 100 μm. Data are presented as means ± SD and were analyzed by a two-tailed *t* test or an ordinary one-way ANOVA followed by Tukey's post hoc test. */#$P < 0.05$, **$P < 0.01$, ***/###$P < 0.001$, and ****$P < 0.0001$. * indicates a significant difference compared with *sparc*$^{-/-}$, and # indicates a significant difference compared with single-drug treatment.

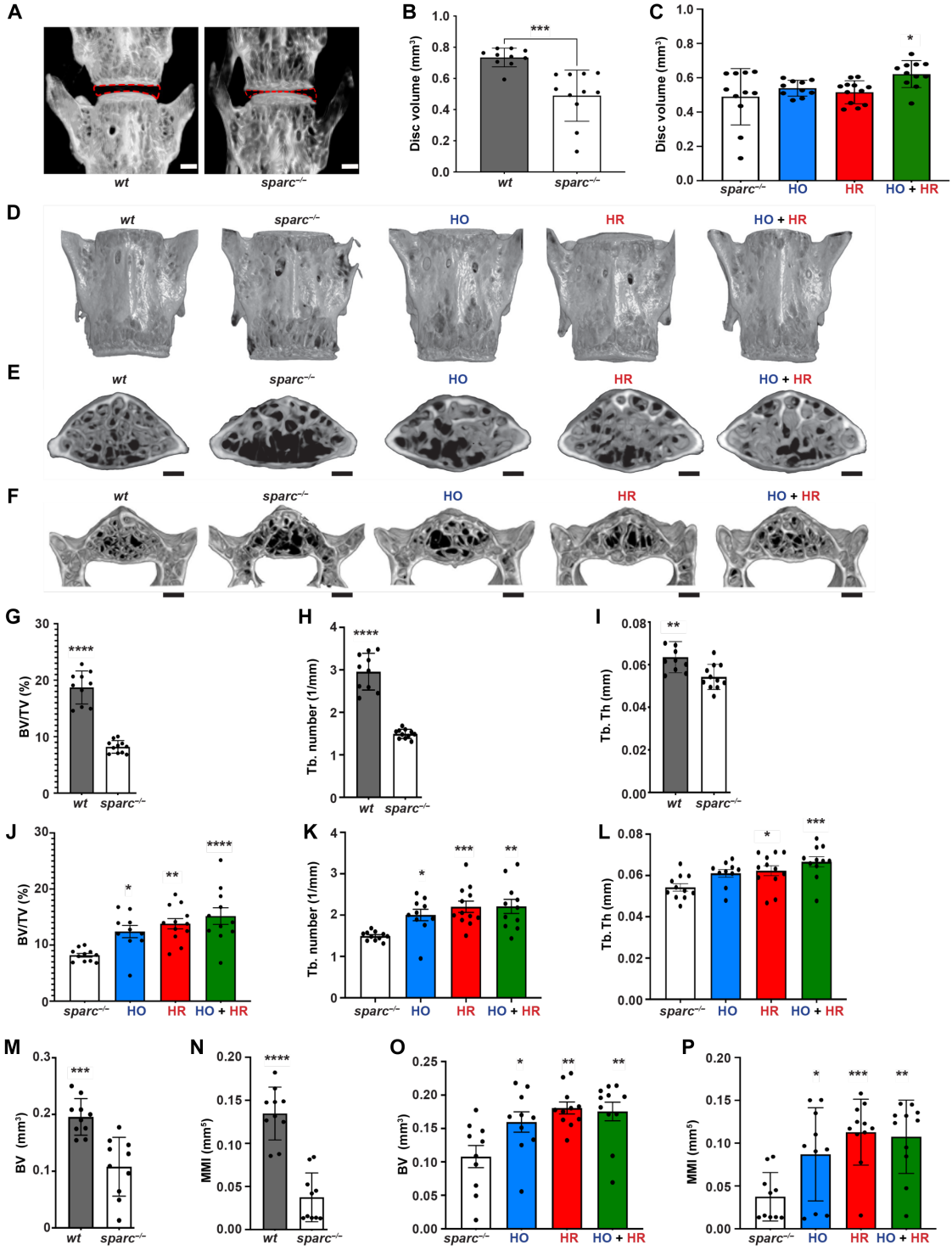

Fig. 6. Treatment with senolytics resulted in increased IVD volume and improved bone quality. (**A**) Representative images showing the difference in disc volume (delineated in red) between 9-month-old *sparc*$^{-/-}$ and wild-type mice. (**B**) Quantification of disc volume showed a lower volume in *sparc*$^{-/-}$ compared to that in WT mice. (**C**) Disc volume of *sparc*$^{-/-}$ IVDs from animals treated with senolytics or vehicle. Representative micro-CT images showing (**D**) vertebrae and (**E** and **F**) trabecular and cortical bone of wild-type and *sparc*$^{-/-}$ mice (vehicle and treated). Quantification of trabecular (**G** to **L**) and cortical (**M** to **P**) bone parameters. Scale bars (A, E, and F), 500 μm. Statistical comparisons were calculated using a two-tailed *t* test or an ordinary one-way ANOVA, with a Dunnett's post hoc analysis as appropriate. Data are presented as means ± SD. **P* < 0.05, ***P* < 0.01, ****P* < 0.001, and *****P* < 0.0001. * indicates a significant difference compared with *sparc*$^{-/-}$. *n* = 10 to 12 animals (3 to 6 males and 5 to 8 females) per group and 3 levels per animal (L4-S1).

Together, this prompted us to evaluate whether the drugs can reduce LBP in a preclinical animal model. First, we validated that the *sparc*$^{-/-}$ mouse model, which is characterized by progressive IVD degeneration and LBP, would be a suitable model to evaluate senolytic treatment (*55*). Our results confirmed previous studies showing a higher degeneration level in knockout compared to that in the wild-type mice (*55*, *56*, *59*, *84*). Using the *p16*^{Ink4a} senescence marker, we found a higher density of senescent IVD cells in *sparc*$^{-/-}$ compared to those in age-matched wild-type animals, which was positively correlated with the degree of IVD degeneration. The observed increase in cellular senescence was further confirmed by higher mRNA expression of genes involved in cellular senescence and SASP factors in *sparc*$^{-/-}$ mice. We compared our data to the MSigDB, Reactome, and SenMayo gene panels developed to identify senescence and SASP factors (*85*–*87*) and found all significantly enriched in *sparc*$^{-/-}$ mice. In addition, *sparc*$^{-/-}$ IVDs released elevated levels of SASP factors. In previous studies, SPARC has been shown to affect senescence and tumorigenesis, with overexpression of SPARC linked to an increase in SnCs in trabecular bone, in fibroblasts, and in enhanced tumor progression (*88*–*92*). In contrast, our findings demonstrate higher levels of senescence markers, SASP expression, and release in *sparc*$^{-/-}$ IVDs and spinal cord, supporting this animal model for the evaluation of senotherapeutics in the context of IVD-related LBP. SnCs are heterogeneous with tissue and species-specific phenotypes; therefore, before venturing into in vivo experiments, we confirmed that *o*-vanillin and RG-7112 could reduce SASP factor release from mouse IVDs ex vivo. The experiments showed a reduction in most (10 of 13) of the tested SASP factors. The panel of SASP factors that we evaluated is described as key factors up-regulated in SnCs where they contribute to paracrine senescence (*3*, *13*, *93*, *94*).

sparc$^{-/-}$ mice develop age-related LBP that is well established at 7 months of age (*54*–*56*, *60*). We chose this time point to evaluate whether systemic treatment with *o*-vanillin and RG-7112 reduced behavioral signs of LBP, SASP factor release, SnCs, and IVD degeneration. We further investigated whether a combination treatment could improve outcomes. We treated the animals orally over 8 weeks and found a significant reduction in pain behavior as determined by a reduction in axial discomfort and mechanical sensitivity. At the termination of the full 8 weeks of treatment, lower pain sensitivity was measured in all the behavioral tests with the combination at a higher dose being the most efficient. Together, the results suggest that senolytics have the potential to reduce behavioral signs of LBP. Other recent reports have demonstrated that genetic and pharmacological elimination of SnCs can improve osteoarthritis (OA) pain and delay age-related IVD degeneration (*95*–*97*).

LBP could, in part, be triggered by SASP factors released from the IVD that could potentially be reduced if the drugs reach and kill SnCs in the IVD. Our results showed that senolytic treatment reduced the release of CXCL-1, CXCL-5, CXCL-9, and CXCL-10. These chemokines have been suggested to induce ECM degradation, inflammatory response (*50*, *98*–*100*), and senescence (*13*, *101*). For example, CXCL-5 promoted cellular senescence in mouse embryos resulting in implantation failure by inducing suppression of cell proliferation in trophoblast cells (*98*). In addition, microarray analysis on AF tissues from discs of aged mice treated with the senolytic drugs D + Q showed down-regulation of CXCL-5 gene expression (*25*). Release of the chemokines CCL-2 and CCL-7 were also reduced by *o*-vanillin and RG-7112 treatment. Elevated expression of them has previously been reported in cells from degenerating IVDs (*50*, *51*, *100*). Additionally, CCL-2 has been reported to play a crucial role in macrophage recruitment and in matrix remodeling in rheumatoid arthritis (*102*). *o*-Vanillin and RG-7112 treatment also reduced cytokines proposed to be secreted by SnCs, including IL-1β, TNF-α, IL-2, IL-10, and IL-6. These factors are widely recognized as important mediators of paracrine senescence in IVD degeneration and OA (*3*, *7*, *13*, *94*, *103*–*113*). Moreover, VEGF-α, a SASP factor that promotes vascular infiltration, was reduced. A positive correlation and co-expression of VEGF and the senescence marker p53 have been demonstrated to promote neovascular infiltration related to IVD degeneration (*114*). Analysis of circulating SASP factors showed no significant systemic difference between *wt* and *sparc*$^{-/-}$ mice.

Our previous work showed an effective reduction of SnCs in response to *o*-vanillin and RG-7112 treatment of human IVD in ex vivo and in vitro systems (*49*, *50*). Here, we could verify that oral treatment resulted in a reduced senescence burden and improved IVD tissue health in *sparc*$^{-/-}$ mice. Previous data from other groups reported a protective effect of reducing senescence with quercetin and ABT263 in injury-induced IVD degeneration in rats (*109*, *115*). Similarly, selective removal of *p16*^{Ink4a}-positive cells in p16-3MR transgenic mice reduced age-related IVD degeneration (*48*), and removal of *p16*^{Ink4a} reduced apoptosis and attenuated SASP in mice following conditional deletion of *p16*^{Ink4a} in the disc (*81*).

Similarly to our results, senolytic combination treatment of D + Q is more efficient in the treatment of idiopathic fibrosis, diabetic kidney disease, and age-related diseases such as bone loss, physical dysfunction, and shortening health span and life span (*27*, *116*–*118*). Weekly injection of D + Q also decreases the senescence burden in age-dependent IVD degeneration (*25*). The beneficial effect of reducing senescence burden and IVD degeneration in our middle-aged animals suggests that *o*-vanillin, RG-7112, and their combination can slow or prevent IVD degeneration. Together, our data suggest that *o*-vanillin and RG-7112 significantly reduce SnCs and SASP factor release when administrated systemically with a combination of the two senolytics, further improving the beneficial effects.

sparc$^{-/-}$ mice start showing behavioral signs of LBP at 4 months of age and would have experienced pain for 3 months before we started the treatment with *o*-vanillin and RG-7112 (*55*). Cellular senescence in various cell types in the CNS has been implicated in the pathogenesis of diseases featuring pain such as osteoarthritis (*50*, *96*, *119*, *120*). An accumulation of SnCs has been reported in neurons (*74*, *76*, *121*), glial cells (*73*, *76*, *77*, *122*–*124*), and astrocytes (*125*–*129*) in humans and animals with pain. Previous studies have also linked SASP and elevated senescence in astrocytes and microglia to pain (*122*, *130*, *131*). Spinal microglia are suggested to contribute to the development of chronic pain, while astrocytes contribute to the maintenance of chronic pain (*78*, *132*, *133*). SnCs accumulate in neurons and the spinal cord and contribute to aging and neurodegenerative diseases. DNA damage, oxidative stress, and mitochondrial dysfunction are key drivers of neuronal and glial senescence. This leads to cellular dysfunction, increased production of SASP factors, and disruption of the neuronal environment (*134*–*136*). Astrocytes, microglia, oligodendrocytes, and neurons can also undergo stress-induced senescence marked by increased oxidative stress, decreased mitochondrial activity, and secretion of pro-inflammatory factors (*137*–*149*). The associated SASP exacerbates neurodegeneration and tissue dysfunction (*136*, *150*, *151*). Targeting

SnCs with senolytics presents a potential therapeutic strategy to reduce neurodegenerative progression and improve glial cell function. We found higher expression of senescence in the dorsal horn of the spinal cord in *sparc*$^{-/-}$ mice, which was reduced by both single and combination treatment. An accumulation of SnCs with age has also been reported in the spinal cord of p16 reporter mice (*152*), with an observed attenuation of the neuroinflammatory phenotype following the suppression of cells expressing *p16*^{Ink4a} (*130*). A correlation between senescence in the spinal cord and nerve injury-associated symptoms has also been described where anti-hyperalgesic and anxiolytic activity was reduced after treatment with the senomorphic rosmarinic acid (*122*). We previously reported an increase in immunoreactivity for the sensory neuropeptide CGRP, the astrocyte marker GFAP, and the microglia marker CD11b in the dorsal horn of the spinal cord in *sparc*$^{-/-}$ mice when compared to that in wild-type mice (*58*, *60*, *67*). In this study, we investigated pain-related neuroplastic changes in the dorsal horn of *sparc*$^{-/-}$ mice treated with senotherapeutics. Depletion of SnCs in the spinal cord of treated mice was accompanied by decreased immunoreactivity for CGRP, GFAP, and CD11b, which could reflect decreased peripheral nociceptive signaling or a decrease in spinal neuron activity. Our results are consistent with the findings of *Du* et al., correlating astrocytic senescence, neuroinflammation at the spinal level, and signs of neuropathic pain resulting from sciatic nerve injury that was reduced by treatment with D + Q (*127*).

sparc$^{-/-}$ mice are known to have osteopenia, which is also a potential contributor to LBP. Recent studies report that senolytic drugs have the potential to improve age-related bone loss in some models (*28*, *115*, *116*). Our results showed that IVD volume and vertebral bone quality could be improved by *o*-vanillin and RG-7112 treatment. Similar to our findings, ABT263 or D + Q demonstrated beneficial effects on bone remodeling in aged mice by lowering bone resorption, enhancing cortical, and maintaining trabecular bone formation (*116*, *153*, *154*). Another study reported greater numbers of senescent osteoclasts in a mouse model of spinal hypersensitivity that was reduced by treatment with ABT263 (*96*). Short-term treatment with ABT263 also showed beneficial effects on bone mass and osteoprogenitor function in aged mice. In addition to decreasing the burden of SnCs, ABT263 treatment decreased trabecular BV/TV and impaired BMSC-derived osteoblasts (*155*). In contrast, senolytic combination treatment with D + Q did not improve the vertebral bone quality of aged mice (*25*).

o-Vanillin, the main metabolite of curcuma, has previously been evaluated as an anti-inflammatory in animal models where it showed a strong safety profile (*156*, *157*). An explorative toxicology study where mice were treated orally 5 days a week for 2 weeks with *o*-vanillin (60 mg/kg) found no sign of treatment-related toxicity (*68*). Similarly, our results showed no cytotoxicity or adverse effects caused by weekly treatment of *o*-vanillin (100 mg/kg) over an 8-week period. RG7112 was the first MDM2 inhibitor to enter clinical trials. Severe adverse effects were common when daily high doses needed to treat cancer were administered to patients with advanced solid tumors and hematological neoplasms (NCT00559533 and NCT00623870) (*69*). Here, we used comparably much lower concentrations and found no effect in weight, mortality, or distance traveled between untreated and animals treated with RG7112 alone or in combination with *o*-vanillin. Together, this indicates that the doses needed to target senescence are safe, although this must be confirmed in a full toxicological study (*68*–*70*). We measured the PK parameters of *o*-vanillin and RG-7112 in mice. We observed typical PK profiles for orally administered compounds, albeit with key differences in bioavailability, distribution, and clearance rates. Senolytics generally exhibit varied absorption and distribution depending on their target tissues, with some, like dasatinib, showing rapid clearance and others, like quercetin, exhibiting prolonged half-lives due to tissue accumulation (*158*–*162*). *o*-Vanillin's high clearance rate and large volume of distribution suggest rapid systemic dispersal and elimination. *o*-Vanillin's chemical structure, consisting of an aromatic ring with hydroxyl and aldehyde groups, imparts hydrophobic characteristics contributing to its lipophilicity, potentially allowing it to be stored in fat tissue and released gradually. Its lipophilic nature and substantial volume of distribution suggest that the compound may exhibit good penetrability in brain tissue. In comparison, RG-7112 shows a lower volume of distribution and slower clearance, aligning more closely with traditional small-molecule inhibitors, where moderate tissue distribution and manageable elimination support sustained efficacy at lower doses. While both compounds demonstrate properties valuable for therapeutic applications, further optimization will enhance their clinical efficacy relative to established drugs. There are ongoing clinical trials with the senolytic drugs quercetin, curcumin, UBX0101, RG-7112, digoxin, azithromycin, and fisetin (NCT04946383, NCT04590196, NCT-04129944, NCT00623870, NCT04834557, NCT00285493, and NCT-04210986), evaluating senolytic drug treatment for a variety of age-related disease.

The conversion of treatment doses from mice to humans using the body surface area normalization approach yields an estimated human dose of ~8 mg/kg for *o*-vanillin (from the 100 mg/kg dose in mice) and 0.4 mg/kg for RG-7112 (from the 5 mg/kg dose in mice) (*163*). These are feasible doses and suggest the potential for clinical translation based on the safety profile and from comparisons with synthetic and natural senolytics compounds. Weekly at 8 mg/kg or daily at 1.14 mg/kg in humans is comparable to existing senolytic regimens (e.g., navitoclax and dasatinib) and natural senolytics (e.g., quercetin and fisetin) (*79*, *117*, *164*–*167*). Weekly administration offers a potentially more patient-friendly schedule. RG7112, when used at lower doses for targeting cellular senescence, avoids the severe toxicities seen in cancer therapy, supporting its repurposing for age-related conditions. Together, *o*-vanillin and RG7112 show promise as senescence-targeting agents, particularly in combination. Optimizing dosing and frequency to ensure safety will be critical for translation to human therapies. Furthermore, various targeted and advanced delivery strategies could be explored. Strategies such as nanotechnology-based systems (e.g., lipid-based carriers and molecular conjugates), cyclodextrin complexes, salt formation, and prodrug design could enhance stability and compatibility while ensuring precise drug delivery and minimizing off-target effects. Emerging technologies, including artificial intelligence, 3D printing, and biopolymer carriers, provide additional opportunities to optimize drug design and delivery. The integration of these approaches and larger animal models (*168*) holds substantial potential to improve the therapeutic efficacy of both compounds. The findings presented in this study show that systemic oral treatment with RG-7112 and *o*-vanillin reduces behavioral indices LBP, reduces SASP, and alleviates degenerative changes in tissues across the spine and spinal cord, with combination treatment resulting in a more robust response. This suggests that senolytics such as *o*-vanillin and RG-7112 could provide novel therapies for treating LBP and other painful disorders where cell senescence is implicated.

MATERIALS AND METHODS

Study design

This study was designed to investigate the potential therapeutic effect of two senolytics (*o*-vanillin and RG-7112) for the treatment of LBP. Initial experiments were designed to determine whether *sparc*$^{-/-}$ mice accumulate SnCs in degenerating lower lumbar IVDs, and the upper lumbar IVDs were used to evaluate the global gene expression profiles of *sparc*$^{-/-}$ and wild-type mice. A second set of IVDs was used to determine SASP factor release and to validate whether *o*-vanillin and RG-7112 reduced SASP release from mouse IVDs ex vivo. We next treated *sparc*$^{-/-}$ mice and evaluated pain behavior. Grip strength and tail suspension tests were used to study axial pain, while the acetone-evoked behavior and von Frey stimulus was used to assess radiating pain. The animals were euthanized, and a multiplex assay was used to quantify SASP factors released from IVDs of treated and untreated animals. A second set of animals was perfused and used to investigate whether the drugs depleted SnCs in the IVDs and spinal cord, and FAST (Fast Green, Alcian Blue, Safranin-O, and tartrazine) staining was used to determine IVD degeneration grade after treatment. Pain signaling in the spinal cord was evaluated with markers of activated astrocytes and microglia in untreated wild-type and treated and untreated *sparc*$^{-/-}$ mice. A third cohort was used to evaluate the effect of senolytic drugs on IVD volume and bone health.

Animals

All experiments were approved by the Animal Care Committee of McGill University following the Canadian Council of Animal Care guidelines (MUHC-10007). Age-matched male and female C57BL/6N (wild-type) and *sparc*$^{-/-}$ mice were used to carry out all experiments. *sparc*$^{-/-}$ mice were developed on a C57BL/6x129SVJ background as previously described (*56*, *169*). Mice were backcrossed and housed in a temperature-controlled room with a 12-hour light/dark cycle, two to five per ventilated polycarbonate, cage (Allentown), and with corncob bedding (Envigo), cotton nesting squares, ad libitum access to food (global soy protein-free extruded rodent diet, irradiated), and water. Sample size was based on previous studies to detect differences between strains and potential pharmacological effects in *sparc*$^{-/-}$ mice (*55*, *56*, *58*, *60*, *67*, *170*).

Ex vivo evaluations

Ex vivo treatment of IVDs

To evaluate whether *o*-vanillin and RG-7112 can target SnCs mouse IVD cells and reduce SASP factors, isolated IVDs were treated in culture ex vivo with single or combined treatments. Nine-month-old *sparc*$^{-/-}$ and wild-type mice were euthanized, and four discs (L1-L5) with a cartilaginous end plate and no bony end plate were excised. *sparc*$^{-/-}$ discs were cultured for 48 hours in Dulbecco's modified eagle medium (DMEM) with 1× GlutaMAX, penicillin (10 U/ml), and streptomycin (10 μg/ml) and one of the following senolytics: 100 μM *o*-vanillin (HO), 5 μM RG-7112 (HR), 100 μM *o*-vanillin and 5 μM RG-7112 (HO + HR), 100 μM *o*-vanillin and 2.5 μM RG-7112 (HO + LR), 50 μM *o*-vanillin and 5 μM RG-7112 (LO + HR), or 50 μM *o*-vanillin and 2.5 μM RG-7112 (LO + LR). The disc medium was changed after 48 hours of treatment and replaced with DMEM with 1× GlutaMAX, penicillin (10 U/ml), and streptomycin (10 μg/ml), which was then collected and used for protein analysis. Similarly, wild-type discs were cultured for 48 hours, with DMEM with 1× GlutaMAX, penicillin (10 U/ml), and streptomycin (10 μg/ml; without senolytics) followed by a medium change at the 48-hour time point. The measure of the selected SASP factors release was performed using Luminex multiplex assay as described below.

In vivo evaluations

Randomization and blinding

Animals were randomly assigned to each treatment group. Experimenters were blinded to genotype and treatment for all experiments and data analysis.

Selection of start and endpoints

The selection of treatment frequency and endpoints was based on previous studies and pilot experiments (*55*, *56*, *58*, *60*, *67*, *170*). The start point of treatment was selected based on pain phenotype and IVD degeneration status. *sparc*$^{-/-}$ mice have established back pain and IVD degeneration at 7 months of age that gets progressively getting worse (*54*–*56*, *60*, *67*). We aimed to determine a potential protective or regenerative effect of the senolytics either alone or as a combination treatment.

Animals and treatment

Seven-month-old male and female mice were randomized into treatment groups. Drug doses were selected extrapolated from ex vivo studies by converting the highest optimal concentration in culture (in micromolar) to the highest dose in vivo (in milligrams per kilogram). Experimenters were blinded to the treatment groups for all experiments. *sparc*$^{-/-}$ and wild-type mice underwent oral gavage every week for 2 months. *sparc*$^{-/-}$ mice received either *o*-vanillin at 100 mg/kg (HO), RG-7112 at 5 mg/kg (HR), *o*-vanillin at 100 mg/kg and RG-7112 at 5 mg/kg (HO + HR), *o*-vanillin at 100 mg/kg and RG-7112 at 2.5 mg/kg (HO + LR), *o*-vanillin at 50 mg/kg and RG-7112 at 5 mg/kg (LO + HR), *o*-vanillin at 50 mg/kg and RG-7112 at 2.5 mg/kg (LO + LR), or vehicle (0.01% dimethyl sulfoxide in saline) as a control. All wild-type mice underwent oral gavage with vehicle control.

Bulk RNA-seq and analysis

Total RNA was extracted (QIAGEN RNeasy kit) and assessed for quality (2100 Bioanalyzer, Agilent) before undergoing bulk RNA-seq analysis, generating 25 million paired-end reads (PE100) per sample on the NovaSeq 6000 platform. Raw data quality was initially evaluated using FastQC (Galaxy version 0.74+galaxy0), and subsequent Trimmomatic (Galaxy version 0.39+galaxy0) was used for adapter trimming and the removal of Illumina-specific sequences. HISAT2 (Galaxy version 2.2.1+galaxy1) was used for read alignment to the mm10 reference genome, and gene expression quantification was performed using featureCounts (Galaxy version 2.0.3+galaxy2). Differential gene expression analysis was conducted using Limma-voom (Galaxy version 3.50.1+galaxy0) with Benjamini-Hochberg–adjusted *P* values to control the false discovery rate. All processes on the Galaxy platform were using default parameters. A 3D PCA plot was generated in R to visualize sample relationships using the scatterplot3d package. GSEA was performed with custom gene sets from MSigDB. Multiple GSEA figures were created in R using the ggplot2, plyr, grid, and gridextra packages. Heatmap visualization of selected senescence-associated genes was created using the R package heatmap.

Pain behavior

Pain behavior was performed as was previously described in our laboratory (*55*, *56*, *58*, *60*, *67*, *170*). All mice were tested in a dedicated behavioral testing room with regular indoor lighting between 8:00 a.m. and 12:00 p.m. Mice were habituated to the room for

1 hour and to Plexiglas testing boxes on a metal grid for another hour (when applicable). The protocol for behavioral testing has been meticulously prepared and validated to minimize stress and handling in the animals (*54*–*56*, *60*, *171*). Each behavioral test lasts between 30 s and 5 min per animal. The animals were subjected to one test per day, except for the first day when von Frey and acetone were tested back to back. When von Frey and acetone were tested back to back, they were performed in the same apparatus, and both tests were based on non-nociceptive infraluminal stimuli (von Frey cut-off, 4 g). The animals were systematically observed for any signs of discomfort or excessive stress before being returned to the animal facility. Grip strength (axial discomfort), acetone-evoked behavior, and mechanical sensitivity to von Frey filaments (radicular pain) were assessed on nontreatment days biweekly. The tail suspension test (axial discomfort) and distance traveled in an open field (motor ability and anxiety-like behavior) were measured every 4 weeks, while mice weighing was performed every 2 weeks.

Grip strength

Axial discomfort was measured with a grip strength meter (Stoelting Co.) by allowing the mice to grip a bar with their forepaws and stretching them by pulling on their tail. The force at which they released was recorded in grams (*172*). In a session, grip strength was measured two to three times and then averaged. Mice were returned to their home cages for ~15 min between measurements.

Acetone-evoked behavior test for cold sensitivity

Behavioral reaction to a cold stimulus was used for radiating leg pain. Acetone (30 to 50 μl) was applied to the left and right hind paws, and the total time of evoked behavior (paw lifting, shaking, and scratching) was recorded for 30 s (*172*).

von Frey test for mechanical sensitivity

von Frey filaments (Stoelting Co.) were applied to the left and right hind paw plantar surfaces until withdrawal or for a total of 5 s, whichever came first (*56*). Stimuli intensity ranged from 0.6 to 4.0 g, corresponding to filament numbers 3.22, 3.61, 3.84, 4.08, and 4.17. The 50% withdrawal threshold in grams was calculated using the up-down method (*173*).

Tail suspension assay

Mice were individually suspended by the tail underneath a platform. Adhesive tape was used on two points to attach the tail (0.5 to 1 cm from the base and the tip of the tail) to the platform and was videotaped for 3 min. The duration of time spent in (i) immobility (not moving but stretched out), (ii) rearing (trying to reach the underside of the platform), (iii) full extension (actively reaching for the floor), and (iv) self-supported (holding either the base of its tail or the tape) was analyzed by a blinded observer using digital software (Labspy, Montreal, QC) over the entire testing period.

Open field

Mice were placed in a 24 cm–by–24 cm Plexiglas enclosure for 5 min. Mice were video recorded from above, and the total distance traveled was analyzed using AnyMaze (*55*).

Luminex multiplex assay

SASP factor release was measured using the Luminex multiplex assay (PPX-15-MXGZF4V). Ex vivo IVD samples were prepared and collected as described in the ex vivo treatment of IVDs section. In vivo IVD samples were obtained following treatment with senolytic compounds from *sparc*$^{-/-}$ and wild-type mice as described in the ex vivo treatment of IVDs section. Fifteen proteins were analyzed according to the manufacturer's instructions. Concentrations (in picograms per milliliter) (IFN-γ, TNF-α, IL-1β, IL-2, IL-6, IL-10, CCL-2, CCL-7, CXCL-1, CXCL-5, CXCL-9, CXCL-10, M-CSF, RANKL, and VEGF-α) were measured in 40 μl of medium. Median fluorescence intensity from microspheres was acquired with a BD FACSCanto II and analyzed in FlowCytomix Pro2.2.1 software (eBioscience). The concentration of each analyte was obtained by interpolating fluorescence intensity to a seven-point dilution standard curve supplied by the manufacturer.

Circulating SASP factor analysis

Blood was collected via cardiac puncture post-euthanasia and centrifuged at 1500*g* for 15 min at 4°C to separate the plasma. The isolated plasma was then stored at −80°C until further analysis. Levels of SASP factors were analyzed using the ProcartaPlex 10-Plex Mouse Kit (Thermo Fisher Scientific, USA) and analyzed with the ProcartaPlex Analysis App, following the manufacturer's protocols.

Histological analysis

Sample preparation. Animals were deeply anesthetized by an intraperitoneally administered mixture of ketamine (100 mg/kg), xylazine (10 mg/kg), and acepromazine (3 mg/kg) and perfused through the left cardiac ventricle with vascular rinse followed by 200 ml of 4% paraformaldehyde in 0.1 M phosphate buffer (pH 7.4), at room temperature, for 20 min. The T13-S1 spinal segment was collected post-perfusion and kept in fixative overnight at 4°C and then decalcified by immersion in 4% ethylenediaminetetraacetic acid in phosphate-buffered saline (PBS) at 4°C for 14 days. The samples were cryoprotected in 30% sucrose in PBS for 4 days at 4°C and embedded in an optimal cutting temperature cutting medium (Tissue-Tek, Sakura Finetek, Torrance, CA, USA). Sixteen-micrometer-thick cryostat (Leica CM3050S, Leica Microsystems Inc., Concord, Ontario, Canada) sections were cut in the sagittal plane, thaw mounted onto gelatin-coated slides, and stored at −20°C.

FAST staining. Staining was performed as described by Millecamps *et al.* (*54*–*56*, *58*, *60*, *67*, *170*). This staining was adapted from the FAST method for colorimetric histologic staining described by Leung *et al.* (*174*) for IVDs. The FAST profile identifies IVD compartments and detects matrix remodeling within the disc. The procedure consists of consecutive baths in (i) acidic Alcian Blue (Sigma-Aldrich, no. A5268), 10 min; (ii) Safranin-O (Sigma-Aldrich, no. S2255), 2.5 min; (iii) 50% ethanol, 1 min; (iv) tartrazine (Sigma-Aldrich, no. HT3028), 10 s; and (v) Fast Green (Sigma-Aldrich, no. F7252), 5 min. After drying, slides were mounted with dibutylphthalate polystyrene xylene (Sigma-Aldrich, USA). IVD degeneration severity grading scale: Grade 0: Healthy IVDs display intact structure, a clear distinction between outer AF and inner NP and negatively charged proteoglycans; grade 1: The changes in extracellular components and IVD integrity were identified as grade 0, normal structure, but the loss of proteoglycans in inner NP; grade 2: internal disruption (loss of boundary) between NP and AF; grade 3: bulging of NP in dorsal aspect; and grade 4: herniation. Each value represents the average grading score of 3 to 4 IVDs per animal.

Spine immunofluorescent histochemistry

Samples were prepared as described under the "Histological analysis, Sample preparation" section. Sagittal sections (three per animal) were incubated for 1 hour at room temperature in a blocking buffer containing 0.3% Triton X-100, 1% bovine albumin, 1% normal donkey serum, and 0.1% sodium azide in PBS. Slides were then incubated with recombinant anti-CDKN2A/*p16*^{Ink4a} antibody (1:100; Abcam, ab211542) in blocking buffer overnight at 4°C, washed three times for 5 min with PBS, and incubated for 1.5 hours at room temperature with secondary antibody (donkey anti-rabbit Cy3, catalog

no. 711-165-152) in blocking buffer. DAPI (1:50,000 in PBS; Sigma-Aldrich) was briefly applied (5 min), and slides were washed thrice for 5 min. Coverslips were mounted using Aqua-Poly/Mount (Polysciences Inc.). Images were taken at ×10 magnification using an Olympus BX51 microscope equipped with an Olympus DP71 camera (Olympus). $p16^{Ink4a}$ and DAPI images were merged using ImageJ, and the percentage of $p16^{Ink4a}$-positive cells was obtained by counting the total number of $p16^{Ink4a}$-positive cells over the total number of cells (DAPI counterstain). An average of ~5000 cells was counted per treatment group. Image analysis was performed by an experimenter blind to strain and treatment groups.

Spinal cord immunofluorescent histochemistry

Spinal cords were harvested following perfusion and euthanasia and fixed in 4% paraformaldehyde for 24 hours at 4°C, followed by cryoprotection using 30% sucrose solution for 24 hours at 4°C. Samples were embedded in blocks of six spinal cords in optimum cutting temperature medium (Tissue-Tek). Sixteen-micrometer-thick cryostat (Leica CM3050S) sections were thaw mounted on gel-coated slides and stored at 20°C until use. Three sections per animal were randomly selected, spanning the lumbar spinal cord for each antibody. Sections were incubated for 1 hour at room temperature in a blocking buffer containing 0.3% Triton X-100, 1% bovine albumin, 1% normal donkey serum, and 0.1% sodium azide in PBS. Slides were then incubated with either recombinant anti-CDKN2A/$p16^{Ink4a}$ antibody (1:100; Abcam, catalog no. ab211542), sheep anti-CGRP polyclonal antibody (1:1000; Enzo Life Sciences, catalog no. BML-CA11370100, lot no. 0807B74), goat anti-GFAP polyclonal antibody (1:1000; Sigma-Aldrich, catalog no. SAB2500462, lot no. 747852C 2G2), or rat monoclonal anti-CD11b antibody (1:1000; Bio-Rad, catalog no. MCA711G, lot no. 0614) in blocking buffer overnight at 4°C; washed three times for 5 min in PBS; and incubated for 1.5 hours at room temperature with appropriate donkey-derived secondary antibodies from Jackson ImmunoResearch: donkey anti-sheep Cy3, catalog no. 713-165-147; donkey anti-goat Alexa Flour 594, catalog no. 705-85-144; donkey anti-rat Alexa Fluor 488, catalog no. 712-225-153; donkey anti-rabbit Alexa Fluor 488, catalog no. 711-545-152; and donkey anti-rabbit Cy3, catalog no. 711-165-152 in blocking buffer. DAPI (1:50,000 in water; Sigma-Aldrich) was briefly applied, and slides were washed another three times for 5 min. Coverslips were mounted using Aqua-Poly/Mount (Polysciences Inc.). Images were taken at ×10 magnification using an Olympus BX51 microscope equipped with an Olympus DP71 camera (Olympus). Using ImageJ, an ROI was drawn around the dorsal horn, and a threshold was established to differentiate between positive immunoreactivity (ir) and background. The percent area of the ROI at or above the threshold was quantified to measure $p16^{Ink4a}$-ir, CGRP-ir, GFAP-ir, or CD11b-ir. The average percent area immunoreactivity across the three sections from each animal was averaged and used as the value for that mouse. Image analysis was performed by an experimenter blind to strain and treatment group.

Micro-CT analysis

Micro-CT scans and analysis were performed as previously described (*28*, *175*). High-resolution scans of fixed spines were conducted from the L4-S1 levels to evaluate the 3D structure. The scans were acquired with a spatial resolution of 15 μm using a Skyscan 1172 micro-CT (Bruker, Kontich, Belgium). This device was equipped with a 0.5-mm aluminum filter and operated at 45-kV voltage, 220-μA current, and a 360° rotation. Image data were captured with a 0.4° increment between rotations and an average of four frames per image, each with an exposure time of 1.46 s. Image reconstruction was performed using the nRecon program (version 1.7.1.0, Bruker), and subsequent analysis was carried out using CTan (version 1.18.8.0, Bruker). CTVOX analysis software (version 3.3, Bruker) was used for the visualization of bone remodeling. The transverse cross-sectional images were then assessed for disc volume parameters and the trabecular and cortical bone morphology. Disc volume was determined by delineating an ROI that involved marking the boundary between the two adjacent end plates. In the case of trabecular analysis, an ROI was selected by defining the boundary between the end plate and transverse process within the vertebral body, with the reference area situated. The 3D datasets were examined to determine BV/TV, Tb. Th, Tb. N, and Tb. Sp. For the evaluation of cortical bone characteristics, 2D assessments were conducted to ascertain cortical BV, Cs. Th, and polar MMI.

Statistical analyses

Power analysis was set with a margin error α of 0.05, a confidence level of 95%, and a 50% response distribution. Power analysis determined a sample size of 8 to 10 wild-type and 8 to 10 $sparc^{-/-}$ animals to observe significant differences (10 to 15 if sex differences become apparent). Data were analyzed using GraphPad Prism 9, with $P \leq 0.05$ being considered statistically different. Data are presented as means ± SD. Data were assessed by two-tailed unpaired *t* tests, repeated-measures one-way analysis of variance (ANOVA), or repeated-measure two-way ANOVA followed by Dunnett's or Tukey's post hoc tests as appropriate.

Supplementary Materials

The PDF file includes:

Figs. S1 to S6
Tables S1 to S16
Legends for movies S1 to S5
Legend for Supporting Data Values file

Other Supplementary Material for this manuscript includes the following:

Movies S1 to S5
Supporting Data Values file

REFERENCES AND NOTES

1. J. Campisi, Aging, cellular senescence, and cancer. *Annu. Rev. Physiol.* **75**, 685–705 (2013).
2. B. G. Childs, M. Gluscevic, D. J. Baker, R. M. Laberge, D. Marquess, J. Dananberg, J. M. van Deursen, Senescent cells: An emerging target for diseases of ageing. *Nat. Rev. Drug Discov.* **16**, 718–735 (2017).
3. J. M. van Deursen, The role of senescent cells in ageing. *Nature* **509**, 439–446 (2014).
4. O. H. Jeon, C. Kim, R. M. Laberge, M. Demaria, S. Rathod, A. P. Vasserot, J. W. Chung, D. H. Kim, Y. Poon, N. David, D. J. Baker, J. M. van Deursen, J. Campisi, J. H. Elisseeff, Local clearance of senescent cells attenuates the development of post-traumatic osteoarthritis and creates a pro-regenerative environment. *Nat. Med.* **23**, 775–781 (2017).
5. C. Feng, H. Liu, M. Yang, Y. Zhang, B. Huang, Y. Zhou, Disc cell senescence in intervertebral disc degeneration: Causes and molecular pathways. *Cell Cycle* **15**, 1674–1684 (2016).
6. Y. Wang, G. Wang, X. Tan, K. Ke, B. Zhao, N. Cheng, Y. Dang, N. Liao, F. Wang, X. Zheng, Q. Li, X. Liu, J. Liu, MT1G serves as a tumor suppressor in hepatocellular carcinoma by interacting with p53. *Oncogenesis* **8**, 67 (2019).
7. D. Munoz-Espin, M. Serrano, Cellular senescence: From physiology to pathology. *Nat. Rev. Mol. Cell Biol.* **15**, 482–496 (2014).
8. L. Hayflick, P. S. Moorhead, The serial cultivation of human diploid cell strains. *Exp. Cell Res.* **25**, 585–621 (1961).
9. O. Toussaint, P. Dumont, J. F. Dierick, T. Pascal, C. Frippiat, F. Chainiaux, J. P. Magalhaes, F. Eliaers, J. Remacle, Stress-induced premature senescence as alternative toxicological method for testing the long-term effects of molecules under development in the industry. *Biogerontology* **1**, 179–183 (2000).
10. O. Toussaint, E. E. Medrano, T. von Zglinicki, Cellular and molecular mechanisms of stress-induced premature senescence (SIPS) of human diploid fibroblasts and melanocytes. *Exp. Gerontol.* **35**, 927–945 (2000).
11. S. Parrinello, J. P. Coppe, A. Krtolica, J. Campisi, Stromal-epithelial interactions in aging and cancer: Senescent fibroblasts alter epithelial cell differentiation. *J. Cell Sci.* **118**, 485–496 (2005).

12. K. Tominaga, The emerging role of senescent cells in tissue homeostasis and pathophysiology. *Pathobiol. Aging Age Relat. Dis.* **5**, 27743 (2015).
13. J. C. Acosta, A. Banito, T. Wuestefeld, A. Georgilis, P. Janich, J. P. Morton, D. Athineos, T. W. Kang, F. Lasitschka, M. Andrulis, G. Pascual, K. J. Morris, S. Khan, H. Jin, G. Dharmalingam, A. P. Snijders, T. Carroll, D. Capper, C. Pritchard, G. J. Inman, T. Longerich, O. J. Sansom, S. A. Benitah, L. Zender, J. Gil, A complex secretory program orchestrated by the inflammasome controls paracrine senescence. *Nat. Cell Biol.* **15**, 978–990 (2013).
14. G. J. Aan, H. A. Hairi, S. Makpol, M. A. Rahman, S. A. Karsani, Differences in protein changes between stress-induced premature senescence and replicative senescence states. *Electrophoresis* **34**, 2209–2217 (2013).
15. F. Debacq-Chainiaux, C. Borlon, T. Pascal, V. Royer, F. Eliaers, N. Ninane, G. Carrard, B. Friguet, F. de Longueville, S. Boffe, J. Remacle, O. Toussaint, Repeated exposure of human skin fibroblasts to UVB at subcytotoxic level triggers premature senescence through the TGF-β1 signaling pathway. *J. Cell Sci.* **118**, 743–758 (2005).
16. B. G. Childs, M. Durik, D. J. Baker, J. M. van Deursen, Cellular senescence in aging and age-related disease: From mechanisms to therapy. *Nat. Med.* **21**, 1424–1435 (2015).
17. J. L. Kirkland, T. Tchkonia, Cellular senescence: A translational perspective. *EBioMedicine* **21**, 21–28 (2017).
18. H. Thoppil, K. Riabowol, Senolytics: A translational bridge between cellular senescence and organismal aging. *Front. Cell Dev. Biol.* **7**, 367 (2019).
19. F. Al-Mansour, A. Alraddadi, B. He, A. Saleh, M. Poblocka, W. Alzahrani, S. Cowley, S. Macip, Characterization of the HDAC/PI3K inhibitor CUDC-907 as a novel senolytic. *Aging* **15**, 2373–2394 (2023).
20. S. Malayaperumal, F. Marotta, M. M. Kumar, I. Somasundaram, A. Ayala, M. M. Pinto, A. Banerjee, S. Pathak, The emerging role of senotherapy in cancer: A comprehensive review. *Clin. Pract.* **13**, 838–852 (2023).
21. Z. Fan, Y. Tong, Z. Yang, S. Wang, T. Huang, D. Yang, Q. Ni, M. Zhang, D. Li, M. Yang, X. Fan, Inhibitor PF-04691502 works as a senolytic to regulate cellular senescence. *Exp. Gerontol.* **186**, 112359 (2024).
22. Q. Xu, Q. Fu, Z. Li, H. Liu, Y. Wang, X. Lin, R. He, X. Zhang, Z. Ju, J. Campisi, J. L. Kirkland, Y. Sun, The flavonoid procyanidin C1 has senotherapeutic activity and increases lifespan in mice. *Nat. Metab.* **3**, 1706–1726 (2021).
23. L. Zhang, L. E. Pitcher, V. Prahalad, L. J. Niedernhofer, P. D. Robbins, Targeting cellular senescence with senotherapeutics: Senolytics and senomorphics. *FEBS J.* **290**, 1362–1383 (2023).
24. Y. Wu, S. Shen, Y. Shi, N. Tian, Y. Zhou, X. Zhang, Senolytics: Eliminating senescent cells and alleviating intervertebral disc degeneration. *Front. Bioeng. Biotechnol.* **10**, 823945 (2022).
25. E. J. Novais, V. A. Tran, S. N. Johnston, K. R. Darris, A. J. Roupas, G. A. Sessions, I. M. Shapiro, B. O. Diekman, M. V. Risbud, Long-term treatment with senolytic drugs Dasatinib and Quercetin ameliorates age-dependent intervertebral disc degeneration in mice. *Nat. Commun.* **12**, 5213 (2021).
26. Y. Zhu, T. Tchkonia, T. Pirtskhalava, A. C. Gower, H. Ding, N. Giorgadze, A. K. Palmer, Y. Ikeno, G. B. Hubbard, M. Lenburg, S. P. O'Hara, N. F. LaRusso, J. D. Miller, C. M. Roos, G. C. Verzosa, N. K. LeBrasseur, J. D. Wren, J. N. Farr, S. Khosla, M. B. Stout, S. J. McGowan, H. Fuhrmann-Stroissnigg, A. U. Gurkar, J. Zhao, D. Colangelo, A. Dorronsoro, Y. Y. Ling, A. S. Barghouthy, D. C. Navarro, T. Sano, P. D. Robbins, L. J. Niedernhofer, J. L. Kirkland, The Achilles' heel of senescent cells: From transcriptome to senolytic drugs. *Aging Cell* **14**, 644–658 (2015).
27. M. Xu, T. Pirtskhalava, J. N. Farr, B. M. Weigand, A. K. Palmer, M. M. Weivoda, C. L. Inman, M. B. Ogrodnik, C. M. Hachfeld, D. G. Fraser, J. L. Onken, K. O. Johnson, G. C. Verzosa, L. G. P. Langhi, M. Weigl, N. Giorgadze, N. K. LeBrasseur, J. D. Miller, D. Jurk, R. J. Singh, D. B. Allison, K. Ejima, G. B. Hubbard, Y. Ikeno, H. Cubro, V. D. Garovic, X. Hou, S. J. Weroha, P. D. Robbins, L. J. Niedernhofer, S. Khosla, T. Tchkonia, J. L. Kirkland, Senolytics improve physical function and increase lifespan in old age. *Nat. Med.* **24**, 1246–1256 (2018).
28. B. Chen, R. Zhu, H. Hu, M. Zhan, T. Wang, F. Huang, F. Wei, Y. Chai, Z. Ling, X. Zou, Elimination of senescent cells by senolytics facilitates bony endplate microvessel formation and mitigates disc degeneration in aged mice. *Front. Cell Dev. Biol.* **10**, 853688 (2022).
29. Global Burden of Disease Study 2013 Collaborators, Global, regional, and national incidence, prevalence, and years lived with disability for 301 acute and chronic diseases and injuries in 188 countries, 1990-2013: A systematic analysis for the Global Burden of Disease Study 2013. *Lancet* **386**, 743–800 (2015).
30. M. A. Adams, W. C. Hutton, The effect of fatigue on the lumbar intervertebral disc. *J. Bone Joint Surg. Br.* **65**, 199–203 (1983).
31. T. Vos, A. D. Flaxman, M. Naghavi, R. Lozano, C. Michaud, M. Ezzati, K. Shibuya, J. A. Salomon, S. Abdalla, V. Aboyans, J. Abraham, I. Ackerman, R. Aggarwal, S. Y. Ahn, M. K. Ali, M. Alvarado, H. R. Anderson, L. M. Anderson, K. G. Andrews, C. Atkinson, L. M. Baddour, A. N. Bahalim, S. Barker-Collo, L. H. Barrero, D. H. Bartels, M. G. Basanez, A. Baxter, M. L. Bell, E. J. Benjamin, D. Bennett, E. Bernabe, K. Bhalla, B. Bhandari, B. Bikbov, A. B. Abdulhak, G. Birbeck, J. A. Black, H. Blencowe, J. D. Blore, F. Blyth, I. Bolliger, A. Bonaventure, S. Boufous, R. Bourne, M. Boussinesq, T. Braithwaite, C. Brayne, L. Bridgett, S. Brooker, P. Brooks, T. S. Brugha, C. Bryan-Hancock, C. Bucello, R. Buchbinder, G. Buckle, C. M. Budke, M. Burch, P. Burney, R. Burstein, B. Calabria, B. Campbell, C. E. Canter, H. Carabin, J. Carapetis, L. Carmona, C. Cella, F. Charlson, H. Chen, A. T. Cheng, D. Chou, S. S. Chugh, L. E. Coffeng, S. D. Colan, S. Colquhoun, K. E. Colson, J. Condon, M. D. Connor, L. T. Cooper, M. Corriere, M. Cortinovis, K. C. de Vaccaro, W. Couser, B. C. Cowie, M. H. Criqui, M. Cross, K. C. Dabhadkar, M. Dahiya, N. Dahodwala, J. Damsere-Derry, G. Danaei, A. Davis, D. De Leo, L. Degenhardt, R. Dellavalle, A. Delossantos, J. Denenberg, S. Derrett, D. C. D. Jarlais, S. D. Dharmaratne, M. Dherani, C. Diaz-Torne, H. Dolk, E. R. Dorsey, T. Driscoll, H. Duber, B. Ebel, K. Edmond, A. Elbaz, S. E. Ali, H. Erskine, P. J. Erwin, P. Espindola, S. E. Ewoigbokhan, F. Farzadfar, V. Feigin, D. T. Felson, A. Ferrari, C. P. Ferri, E. M. Fevre, M. M. Finucane, S. Flaxman, L. Flood, K. Foreman, M. H. Forouzanfar, F. G. Fowkes, R. Franklin, M. Fransen, M. K. Freeman, B. J. Gabbe, S. E. Gabriel, E. Gakidou, H. A. Ganatra, B. Garcia, F. Gaspari, R. F. Gillum, G. Gmel, R. Gosselin, R. Grainger, J. Groeger, F. Guillemin, D. Gunnell, R. Gupta, J. Haagsma, H. Hagan, Y. A. Halasa, W. Hall, D. Haring, J. M. Haro, J. E. Harrison, R. Havmoeller, R. J. Hay, H. Higashi, C. Hill, B. Hoen, H. Hoffman, P. J. Hotez, D. Hoy, J. J. Huang, S. E. Ibeanusi, K. H. Jacobsen, S. L. James, D. Jarvis, R. Jasrasaria, S. Jayaraman, N. Johns, J. B. Jonas, G. Karthikeyan, N. Kassebaum, N. Kawakami, A. Keren, J. P. Khoo, C. H. King, L. M. Knowlton, O. Kobusingye, A. Koranteng, R. Krishnamurthi, R. Lalloo, L. L. Laslett, T. Lathlean, J. L. Leasher, Y. Y. Lee, J. Leigh, S. S. Lim, E. Limb, J. K. Lin, M. Lipnick, S. E. Lipshultz, W. Liu, M. Loane, S. L. Ohno, R. Lyons, J. Ma, J. Mabweijano, M. F. MacIntyre, R. Malekzadeh, L. Mallinger, S. Manivannan, W. Marcenes, L. March, D. J. Margolis, G. B. Marks, R. Marks, A. Matsumori, R. Matzopoulos, B. M. Mayosi, J. H. McAnulty, M. M. McDermott, N. McGill, J. McGrath, M. E. Medina-Mora, M. Meltzer, G. A. Mensah, T. R. Merriman, A. C. Meyer, V. Miglioli, M. Miller, T. R. Miller, P. B. Mitchell, A. O. Mocumbi, T. E. Moffitt, A. A. Mokdad, L. Monasta, M. Montico, M. Moradi-Lakeh, A. Moran, L. Morawska, R. Mori, M. E. Murdoch, M. K. Mwaniki, K. Naidoo, M. N. Nair, L. Naldi, K. M. Narayan, P. K. Nelson, R. G. Nelson, M. C. Nevitt, C. R. Newton, S. Nolte, P. Norman, R. Norman, M. O'Donnell, S. O'Hanlon, C. Olives, S. B. Omer, K. Ortblad, R. Osborne, D. Ozgediz, A. Page, B. Pahari, J. D. Pandian, A. P. Rivero, S. B. Patten, N. Pearce, R. P. Padilla, F. Perez-Ruiz, N. Perico, K. Pesudovs, D. Phillips, M. R. Phillips, K. Pierce, S. Pion, G. V. Polanczyk, S. Polinder, C. A. Pope III, S. Popova, E. Porrini, F. Pourmalek, M. Prince, R. L. Pullan, K. D. Ramaiah, D. Ranganathan, H. Razavi, M. Regan, J. T. Rehm, D. B. Rein, G. Remuzzi, K. Richardson, F. P. Rivara, T. Roberts, C. Robinson, F. R. De Leon, L. Ronfani, R. Room, L. C. Rosenfeld, L. Rushton, R. L. Sacco, S. Saha, U. Sampson, L. Sanchez-Riera, E. Sanman, D. C. Schwebel, J. G. Scott, M. Segui-Gomez, S. Shahraz, D. S. Shepard, H. Shin, R. Shivakoti, D. Singh, G. M. Singh, J. A. Singh, J. Singleton, D. A. Sleet, K. Sliwa, E. Smith, J. L. Smith, N. J. Stapelberg, A. Steer, T. Steiner, W. A. Stolk, L. J. Stovner, C. Sudfeld, S. Syed, G. Tamburlini, M. Tavakkoli, H. R. Taylor, J. A. Taylor, W. J. Taylor, B. Thomas, W. M. Thomson, G. D. Thurston, I. M. Tleyjeh, M. Tonelli, J. A. Towbin, T. Truelsen, M. K. Tsilimbaris, C. Ubeda, E. A. Undurraga, M. J. van der Werf, J. van Os, M. S. Vavilala, N. Venketasubramanian, M. Wang, W. Wang, K. Watt, D. J. Weatherall, M. A. Weinstock, R. Weintraub, M. G. Weisskopf, M. M. Weissman, R. A. White, H. Whiteford, S. T. Wiersma, J. D. Wilkinson, H. C. Williams, S. R. Williams, E. Witt, F. Wolfe, A. D. Woolf, S. Wulf, P. H. Yeh, A. K. Zaidi, Z. J. Zheng, D. Zonies, A. D. Lopez, C. J. Murray, M. A. AlMazroa, Z. A. Memish, Years lived with disability (YLDs) for 1160 sequelae of 289 diseases and injuries 1990–2010: A systematic analysis for the Global Burden of Disease Study 2010. *Lancet* **380**, 2163–2196 (2012).
32. P. P. Vergroesen, I. Kingma, K. S. Emanuel, R. J. Hoogendoorn, T. J. Welting, B. J. van Royen, J. H. van Dieen, T. H. Smit, Mechanics and biology in intervertebral disc degeneration: A vicious circle. *Osteoarthr. Cartil.* **23**, 1057–1070 (2015).
33. Relieving pain in America: A blueprint for transforming prevention, care, education, and research. *Mil. Med.* **181**, 397–399 (2016).
34. W. T. Crow, D. R. Willis, Estimating cost of care for patients with acute low back pain: A retrospective review of patient records. *J. Am. Osteopath. Assoc.* **109**, 229–233 (2009).
35. H. E. Gruber, J. A. Ingram, H. J. Norton, E. N. Hanley Jr., Senescence in cells of the aging and degenerating intervertebral disc: Immunolocalization of senescence-associated β-galactosidase in human and sand rat discs. *Spine* **32**, 321–327 (2007).
36. C. L. Le Maitre, A. J. Freemont, J. A. Hoyland, Accelerated cellular senescence in degenerate intervertebral discs: A possible role in the pathogenesis of intervertebral disc degeneration. *Arthritis Res. Ther.* **9**, R45 (2007).
37. S. Roberts, E. H. Evans, D. Kletsas, D. C. Jaffray, S. M. Eisenstein, Senescence in human intervertebral discs. *Eur. Spine J.* **15**, 312–316 (2006).
38. K. W. Kim, H. N. Chung, K. Y. Ha, J. S. Lee, Y. Y. Kim, Senescence mechanisms of nucleus pulposus chondrocytes in human intervertebral discs. *Spine J.* **9**, 658–666 (2009).
39. F. Wang, F. Cai, R. Shi, X. H. Wang, X. T. Wu, Aging and age related stresses: A senescence mechanism of intervertebral disc degeneration. *Osteoarthr. Cartil.* **24**, 398–408 (2016).
40. J. Dowdell, M. Erwin, T. Choma, A. Vaccaro, J. Iatridis, S. K. Cho, Intervertebral disk degeneration and repair. *Neurosurgery* **80**, S46–S54 (2017).
41. S. M. Rider, S. Mizuno, J. D. Kang, Molecular mechanisms of intervertebral disc degeneration. *Spine Surg. Relat. Res.* **3**, 1–11 (2019).

42. K. Zhang, Y. Zhang, C. Zhang, L. Zhu, Upregulation of P53 promotes nucleus pulposus cell apoptosis in intervertebral disc degeneration through upregulating NDRG2. *Cell Biol. Int.* **45**, 1966–1975 (2021).
43. P. Silwal, A. M. Nguyen-Thai, H. A. Mohammad, Y. Wang, P. D. Robbins, J. Y. Lee, N. V. Vo, Cellular senescence in intervertebral disc aging and degeneration: Molecular mechanisms and potential therapeutic opportunities. *Biomolecules* **13**, 686 (2023).
44. J. Xu, T. Shao, J. Lou, J. Zhang, C. Xia, Aging, cell senescence, the pathogenesis and targeted therapies of intervertebral disc degeneration. *Front. Pharmacol.* **14**, 1172920 (2023).
45. K. Ngo, P. Patil, S. J. McGowan, L. J. Niedernhofer, P. D. Robbins, J. Kang, G. Sowa, N. Vo, Senescent intervertebral disc cells exhibit perturbed matrix homeostasis phenotype. *Mech. Ageing Dev.* **166**, 16–23 (2017).
46. J. Bedore, A. Leask, C. A. Seguin, Targeting the extracellular matrix: Matricellular proteins regulate cell-extracellular matrix communication within distinct niches of the intervertebral disc. *Matrix Biol.* **37**, 124–130 (2014).
47. H. Che, J. Li, Y. Li, C. Ma, H. Liu, J. Qin, J. Dong, Z. Zhang, C. J. Xian, D. Miao, L. Wang, Y. Ren, p16 deficiency attenuates intervertebral disc degeneration by adjusting oxidative stress and nucleus pulposus cell cycle. *eLife* **9**, e52570 (2020).
48. P. Patil, Q. Dong, D. Wang, J. Chang, C. Wiley, M. Demaria, J. Lee, J. Kang, L. J. Niedernhofer, P. D. Robbins, G. Sowa, J. Campisi, D. Zhou, N. Vo, Systemic clearance of *p16*^{INK4a}-positive senescent cells mitigates age-associated intervertebral disc degeneration. *Aging Cell* **18**, e12927 (2019).
49. H. Cherif, D. G. Bisson, P. Jarzem, M. Weber, J. A. Ouellet, L. Haglund, Curcumin and o-vanillin exhibit evidence of senolytic activity in human IVD cells in vitro. *J. Clin. Med.* **8**, 433 (2019).
50. H. Cherif, D. G. Bisson, M. Mannarino, O. Rabau, J. A. Ouellet, L. Haglund, Senotherapeutic drugs for human intervertebral disc degeneration and low back pain. *eLife* **9**, e54693 (2020).
51. M. Mannarino, H. Cherif, L. Li, K. Sheng, O. Rabau, P. Jarzem, M. H. Weber, J. A. Ouellet, L. Haglund, Toll-like receptor 2 induced senescence in intervertebral disc cells of patients with back pain can be attenuated by o-vanillin. *Arthritis Res. Ther.* **23**, 117 (2021).
52. M. Mannarino, O. Wu-Martinez, K. Sheng, L. Li, R. Navarro-Ramirez, P. Jarzem, J. A. Ouellet, H. Cherif, L. Haglund, Senolytic combination treatment is more potent than single drugs in reducing inflammatory and senescence burden in cells from painful degenerating IVDs. *Biomolecules* **13**, 1257 (2023).
53. E. Krock, D. H. Rosenzweig, A. J. Chabot-Dore, P. Jarzem, M. H. Weber, J. A. Ouellet, L. S. Stone, L. Haglund, Painful, degenerating intervertebral discs up-regulate neurite sprouting and CGRP through nociceptive factors. *J. Cell. Mol. Med.* **18**, 1213–1225 (2014).
54. M. Millecamps, J. T. Czerminski, A. P. Mathieu, L. S. Stone, Behavioral signs of axial low back pain and motor impairment correlate with the severity of intervertebral disc degeneration in a mouse model. *Spine J.* **15**, 2524–2537 (2015).
55. M. Millecamps, M. Tajerian, L. Naso, H. E. Sage, L. S. Stone, Lumbar intervertebral disc degeneration associated with axial and radiating low back pain in ageing SPARC-null mice. *Pain* **153**, 1167–1179 (2012).
56. M. Millecamps, M. Tajerian, E. H. Sage, L. S. Stone, Behavioral signs of chronic back pain in the SPARC-null mouse. *Spine* **36**, 95–102 (2011).
57. H. E. Gruber, E. H. Sage, H. J. Norton, S. Funk, J. Ingram, E. N. Hanley Jr., Targeted deletion of the SPARC gene accelerates disc degeneration in the aging mouse. *J. Histochem. Cytochem.* **53**, 1131–1138 (2005).
58. M. Miyagi, M. Millecamps, A. T. Danco, S. Ohtori, K. Takahashi, L. S. Stone, ISSLS prize winner: Increased innervation and sensory nervous system plasticity in a mouse model of low back pain due to intervertebral disc degeneration. *Spine* **39**, 1345–1354 (2014).
59. H. E. Gruber, J. A. Ingram, K. Leslie, E. N. Hanley Jr., Cellular, but not matrix, immunolocalization of SPARC in the human intervertebral disc: Decreasing localization with aging and disc degeneration. *Spine* **29**, 2223–2228 (2004).
60. E. Krock, M. Millecamps, K. M. Anderson, A. Srivastava, T. E. Reihsen, P. Hari, Y. R. Sun, S. H. Jang, G. L. Wilcox, K. G. Belani, D. S. Beebe, J. Ouellet, M. R. Pinto, L. J. Kehl, L. Haglund, L. S. Stone, Interleukin-8 as a therapeutic target for chronic low back pain: Upregulation in human cerebrospinal fluid and pre-clinical validation with chronic reparixin in the SPARC-null mouse model. *EBioMedicine* **43**, 487–500 (2019).
61. H. Cherif, M. Mannarino, A. S. Pacis, J. Ragoussis, O. Rabau, J. A. Ouellet, L. Haglund, Single-cell RNA-seq analysis of cells from degenerating and non-degenerating intervertebral discs from the same individual reveals new biomarkers for intervertebral disc degeneration. *Int. J. Mol. Sci.* **23**, 3993 (2022).
62. M. C. Whittal, S. Molladavoodi, D. P. Zwambag, M. Millecamps, L. S. Stone, D. E. Gregory, Mechanical consequence of induced intervertebral disc degeneration in the SPARC-null mouse. *J. Biomech. Eng.* **143**, 024501 (2021).
63. Z. Y. Li, A. F. Zhou, G. Li, L. Y. Zhou, P. M. Pu, K. Zhu, Z. Zheng, Y. J. Wang, Q. Q. Liang, M. Yao, X. J. Cui, Chronic spinal cord compression associated with intervertebral disc degeneration in SPARC-null mice. *Neural Regen. Res.* **18**, 634–642 (2023).
64. M. C. Whittal, S. J. Poynter, K. Samms, K. J. Briar, S. I. Sinopoli, M. Millecamps, L. S. Stone, S. J. DeWitte-Orr, D. E. Gregory, TAK-242 treatment and its effect on mechanical properties and gene expression associated with IVD degeneration in SPARC-null mice. *Eur. Spine J.* **31**, 2801–2811 (2022).
65. Y. Kawarai, S. H. Jang, S. Lee, M. Millecamps, H. Kang, S. Gregoire, M. Suzuki-Narita, S. Ohtori, L. S. Stone, Exercise attenuates low back pain and alters epigenetic regulation in intervertebral discs in a mouse model. *Spine J.* **21**, 1938–1949 (2021).
66. S. Gregoire, D. Cheishvili, M. Salmon-Divon, S. Dymov, L. Topham, V. Calderon, Y. Shir, M. Szyf, L. S. Stone, Epigenetic signature of chronic low back pain in human T cells. *Pain Rep.* **6**, e960 (2021).
67. E. Krock, M. Millecamps, J. B. Currie, L. S. Stone, L. Haglund, Low back pain and disc degeneration are decreased following chronic toll-like receptor 4 inhibition in a mouse model. *Osteoarthr. Cartil.* **26**, 1236–1246 (2018).
68. A. Marton, E. Kusz, C. Kolozsi, V. Tubak, G. Zagotto, K. Buzas, L. Quintieri, C. Vizler, Vanillin analogues *o*-vanillin and 2,4,6-trihydroxybenzaldehyde inhibit NFkB activation and suppress growth of A375 human melanoma. *AntiCancer Res.* **36**, 5743–5750 (2016).
69. I. Ray-Coquard, J. Y. Blay, A. Italiano, A. Le Cesne, N. Penel, J. Zhi, F. Heil, R. Rueger, B. Graves, M. Ding, D. Geho, S. A. Middleton, L. T. Vassilev, G. L. Nichols, B. N. Bui, Effect of the MDM2 antagonist RG7112 on the P53 pathway in patients with MDM2-amplified, well-differentiated or dedifferentiated liposarcoma: An exploratory proof-of-mechanism study. *Lancet Oncol.* **13**, 1133–1140 (2012).
70. M. Verreault, C. Schmitt, L. Goldwirt, K. Pelton, S. Haidar, C. Levasseur, J. Guehennec, D. Knoff, M. Labussiere, Y. Marie, A. H. Ligon, K. Mokhtari, K. Hoang-Xuan, M. Sanson, B. M. Alexander, P. Y. Wen, J. Y. Delattre, K. L. Ligon, A. Idbaih, Preclinical efficacy of the MDM2 inhibitor RG7112 in MDM2-amplified and TP53 wild-type glioblastomas. *Clin. Cancer Res.* **22**, 1185–1196 (2016).
71. S. H. Jang, S. Lee, M. Millecamps, A. Danco, H. Kang, S. Gregoire, M. Suzuki-Narita, L. S. Stone, Effect of voluntary running activity on mRNA expression of extracellular matrix genes in a mouse model of intervertebral disc degeneration. *JOR Spine* **4**, e1148 (2021).
72. S. Lee, S. H. Jang, M. Suzuki-Narita, S. Gregoire, M. Millecamps, L. S. Stone, Voluntary running attenuates behavioural signs of low back pain: Dimorphic regulation of intervertebral disc inflammation in male and female SPARC-null mice. *Osteoarthr. Cartil.* **30**, 110–123 (2022).
73. T. J. Bussian, A. Aziz, C. F. Meyer, B. L. Swenson, J. M. van Deursen, D. J. Baker, Clearance of senescent glial cells prevents tau-dependent pathology and cognitive decline. *Nature* **562**, 578–582 (2018).
74. A. M. Nicaise, L. J. Wagstaff, C. M. Willis, C. Paisie, H. Chandok, P. Robson, V. Fossati, A. Williams, S. J. Crocker, Cellular senescence in progenitor cells contributes to diminished remyelination potential in progressive multiple sclerosis. *Proc. Natl. Acad. Sci. U.S.A.* **116**, 9030–9039 (2019).
75. D. Paramos-de-Carvalho, I. Martins, A. M. Cristovao, A. F. Dias, D. Neves-Silva, T. Pereira, D. Chapela, A. Farinho, A. Jacinto, L. Saude, Targeting senescent cells improves functional recovery after spinal cord injury. *Cell Rep.* **36**, 109334 (2021).
76. I. Vazquez-Villasenor, C. J. Garwood, P. R. Heath, J. E. Simpson, P. G. Ince, S. B. Wharton, Expression of p16 and p21 in the frontal association cortex of ALS/MND brains suggests neuronal cell cycle dysregulation and astrocyte senescence in early stages of the disease. *Neuropathol. Appl. Neurobiol.* **46**, 171–185 (2020).
77. P. Zhang, Y. Kishimoto, I. Grammatikakis, K. Gottimukkala, R. G. Cutler, S. Zhang, K. Abdelmohsen, V. A. Bohr, J. Misra Sen, M. Gorospe, M. P. Mattson, Senolytic therapy alleviates Aβ-associated oligodendrocyte progenitor cell senescence and cognitive deficits in an Alzheimer's disease model. *Nat. Neurosci.* **22**, 719–728 (2019).
78. C. I. Svensson, E. Brodin, Spinal astrocytes in pain processing: Non-neuronal cells as therapeutic targets. *Mol. Interv.* **10**, 25–38 (2010).
79. S. Chaib, T. Tchkonia, J. L. Kirkland, Cellular senescence and senolytics: The path to the clinic. *Nat. Med.* **28**, 1556–1568 (2022).
80. N. Vo, H. Y. Seo, A. Robinson, G. Sowa, D. Bentley, L. Taylor, R. Studer, A. Usas, J. Huard, S. Alber, S. C. Watkins, J. Lee, P. Coehlo, D. Wang, M. Loppini, P. D. Robbins, L. J. Niedernhofer, J. Kang, Accelerated aging of intervertebral discs in a mouse model of progeria. *J. Orthop. Res.* **28**, 1600–1607 (2010).
81. E. J. Novais, B. O. Diekman, I. M. Shapiro, M. V. Risbud, p16^{Ink4a} deletion in cells of the intervertebral disc affects their matrix homeostasis and senescence associated secretory phenotype without altering onset of senescence. *Matrix Biol.* **82**, 54–70 (2019).
82. J. L. Kirkland, T. Tchkonia, Senolytic drugs: From discovery to translation. *J. Intern. Med.* **288**, 518–536 (2020).
83. L. I. Prieto, S. I. Graves, D. J. Baker, Insights from in vivo studies of cellular senescence. *Cells* **9**, 954 (2020).
84. A. Ghanemi, M. Yoshioka, J. St-Amand, Secreted protein acidic and rich in cysteine as a regeneration factor: Beyond the tissue repair. *Life* **11**, 38 (2021).
85. A. Liberzon, C. Birger, H. Thorvaldsdottir, M. Ghandi, J. P. Mesirov, P. Tamayo, The Molecular Signatures Database (MSigDB) hallmark gene set collection. *Cell Syst.* **1**, 417–425 (2015).
86. D. Saul, R. L. Kosinsky, E. J. Atkinson, M. L. Doolittle, X. Zhang, N. K. LeBrasseur, R. J. Pignolo, P. D. Robbins, L. J. Niedernhofer, Y. Ikeno, D. Jurk, J. F. Passos, L. J. Hickson,

A. Xue, D. G. Monroe, T. Tchkonia, J. L. Kirkland, J. N. Farr, S. Khosla, A new gene set identifies senescent cells and predicts senescence-associated pathways across tissues. *Nat. Commun.* **13**, 4827 (2022).
87. A. Subramanian, P. Tamayo, V. K. Mootha, S. Mukherjee, B. L. Ebert, M. A. Gillette, A. Paulovich, S. L. Pomeroy, T. R. Golub, E. S. Lander, J. P. Mesirov, Gene set enrichment analysis: A knowledge-based approach for interpreting genome-wide expression profiles. *Proc. Natl. Acad. Sci. U.S.A.* **102**, 15545–15550 (2005).
88. S. A. Arnold, L. B. Rivera, A. F. Miller, J. G. Carbon, S. P. Dineen, Y. Xie, D. H. Castrillon, E. H. Sage, P. Puolakkainen, A. D. Bradshaw, R. A. Brekken, Lack of host SPARC enhances vascular function and tumor spread in an orthotopic murine model of pancreatic carcinoma. *Dis. Model. Mech.* **3**, 57–72 (2010).
89. C. Chiodoni, M. P. Colombo, S. Sangaletti, Matricellular proteins: From homeostasis to inflammation, cancer, and metastasis. *Cancer Metastasis Rev.* **29**, 295–307 (2010).
90. A. Chlenski, S. L. Cohn, Modulation of matrix remodeling by SPARC in neoplastic progression. *Semin. Cell Dev. Biol.* **21**, 55–65 (2010).
91. G. P. Nagaraju, R. Dontula, B. F. El-Rayes, S. S. Lakka, Molecular mechanisms underlying the divergent roles of SPARC in human carcinogenesis. *Carcinogenesis* **35**, 967–973 (2014).
92. N. Said, H. F. Frierson, M. Sanchez-Carbayo, R. A. Brekken, D. Theodorescu, Loss of SPARC in bladder cancer enhances carcinogenesis and progression. *J. Clin. Invest.* **123**, 751–766 (2013).
93. X. He, W. Hu, Y. Zhang, M. Chen, Y. Ding, H. Yang, F. He, Q. Gu, Q. Shi, Cellular senescence in skeletal disease: Mechanisms and treatment. *Cell. Mol. Biol. Lett.* **28**, 88 (2023).
94. M. V. Risbud, I. M. Shapiro, Role of cytokines in intervertebral disc degeneration: Pain and disc content. *Nat. Rev. Rheumatol.* **10**, 44–56 (2014).
95. T. H. Gil, H. Zheng, H. G. Lee, J. W. Shin, S. W. Hwang, K. M. Jang, O. H. Jeon, Senolytic drugs relieve pain by reducing peripheral nociceptive signaling without modifying joint tissue damage in spontaneous osteoarthritis. *Aging* **14**, 6006–6027 (2022).
96. D. Pan, K. G. Benkato, X. Han, J. Zheng, V. Kumar, M. Wan, J. Zheng, X. Cao, Senescence of endplate osteoclasts induces sensory innervation and spinal pain. *eLife* **12**, RP92889 (2024).
97. Y. Saito, M. Miyajima, S. Yamamoto, T. Sato, N. Miura, M. Fujimiya, T. S. Chikenji, Accumulation of senescent neural cells in murine lupus with depression-like behavior. *Front. Immunol.* **12**, 692321 (2021).
98. Y. Kawagoe, I. Kawashima, Y. Sato, N. Okamoto, K. Matsubara, K. Kawamura, CXCL5-CXCR2 signaling is a senescence-associated secretory phenotype in preimplantation embryos. *Aging Cell* **19**, e13240 (2020).
99. C. Liu, H. D. Fei, Z. Y. Sun, J. W. Tian, Bioinformatic analysis of the microarray gene expression profile in degenerative intervertebral disc cells exposed to TNF-α. *Eur. Rev. Med. Pharmacol. Sci.* **19**, 3332–3339 (2015).
100. K. L. Phillips, N. Chiverton, A. L. Michael, A. A. Cole, L. M. Breakwell, G. Haddock, R. A. Bunning, A. K. Cross, C. L. Le Maitre, The cytokine and chemokine expression profile of nucleus pulposus cells: Implications for degeneration and regeneration of the intervertebral disc. *Arthritis Res. Ther.* **15**, R213 (2013).
101. J. P. Coppe, P. Y. Desprez, A. Krtolica, J. Campisi, The senescence-associated secretory phenotype: The dark side of tumor suppression. *Annu. Rev. Pathol.* **5**, 99–118 (2010).
102. N. Maruotti, E. Crivellato, F. P. Cantatore, A. Vacca, D. Ribatti, Mast cells in rheumatoid arthritis. *Clin. Rheumatol.* **26**, 1–4 (2007).
103. S. Ashraf, P. Santerre, R. Kandel, Induced senescence of healthy nucleus pulposus cells is mediated by paracrine signaling from TNF-α-activated cells. *FASEB J.* **35**, e21795 (2021).
104. J. Birch, J. Gil, Senescence and the SASP: Many therapeutic avenues. *Genes Dev.* **34**, 1565–1576 (2020).
105. C. C. Chen, J. Chen, W. L. Wang, L. Xie, C. Q. Shao, Y. X. Zhang, Inhibition of the P53/P21 pathway attenuates the effects of senescent nucleus pulposus cell-derived exosomes on the senescence of nucleus pulposus cells. *Orthop. Surg.* **13**, 583–591 (2021).
106. J. Chen, J. J. Xie, M. Y. Jin, Y. T. Gu, C. C. Wu, W. J. Guo, Y. Z. Yan, Z. J. Zhang, J. L. Wang, X. L. Zhang, Y. Lin, J. L. Sun, G. H. Zhu, X. Y. Wang, Y. S. Wu, Sirt6 overexpression suppresses senescence and apoptosis of nucleus pulposus cells by inducing autophagy in a model of intervertebral disc degeneration. *Cell Death Dis.* **9**, 56 (2018).
107. M. Muller, Cellular senescence: Molecular mechanisms, in vivo significance, and redox considerations. *Antioxid. Redox Signal.* **11**, 59–98 (2009).
108. M. J. Pearson, D. Herndler-Brandstetter, M. A. Tariq, T. A. Nicholson, A. M. Philp, H. L. Smith, E. T. Davis, S. W. Jones, J. M. Lord, IL-6 secretion in osteoarthritis patients is mediated by chondrocyte-synovial fibroblast cross-talk and is enhanced by obesity. *Sci. Rep.* **7**, 3451 (2017).
109. Z. Shao, B. Wang, Y. Shi, C. Xie, C. Huang, B. Chen, H. Zhang, G. Zeng, H. Liang, Y. Wu, Y. Zhou, N. Tian, A. Wu, W. Gao, X. Wang, X. Zhang, Senolytic agent Quercetin ameliorates intervertebral disc degeneration via the Nrf2/NF-κB axis. *Osteoarthr. Cartil.* **29**, 413–422 (2021).
110. N. E. Sharpless, C. J. Sherr, Forging a signature of in vivo senescence. *Nat. Rev. Cancer* **15**, 397–408 (2015).
111. C. Wang, X. Yu, Y. Yan, W. Yang, S. Zhang, Y. Xiang, J. Zhang, W. Wang, Tumor necrosis factor-α: A key contributor to intervertebral disc degeneration. *Acta Biochim. Biophys. Sin.* **49**, 1–13 (2017).
112. Y. Wang, M. Che, J. Xin, Z. Zheng, J. Li, S. Zhang, The role of IL-1β and TNF-alpha in intervertebral disc degeneration. *Biomed. Pharmacother.* **131**, 110660 (2020).
113. J. Xie, B. Li, P. Zhang, L. Wang, H. Lu, X. Song, Osteogenic protein-1 attenuates the inflammatory cytokine-induced NP cell senescence through regulating the ROS/NF-κB pathway. *Biomed. Pharmacother.* **99**, 431–437 (2018).
114. X. Y. Lu, X. H. Ding, L. J. Zhong, H. Xia, X. D. Chen, H. Huang, Expression and significance of VEGF and p53 in degenerate intervertebral disc tissue. *Asian Pac. J. Trop. Med.* **6**, 79–81 (2013).
115. S. Lim, S. B. An, M. Jung, H. P. Joshi, H. Kumar, C. Kim, S. Y. Song, J. R. Lee, M. Kang, I. Han, B. S. Kim, Local delivery of senolytic drug inhibits intervertebral disc degeneration and restores intervertebral disc structure. *Adv. Healthc. Mater.* **11**, e2101483 (2022).
116. J. N. Farr, M. Xu, M. M. Weivoda, D. G. Monroe, D. G. Fraser, J. L. Onken, B. A. Negley, J. G. Sfeir, M. B. Ogrodnik, C. M. Hachfeld, N. K. LeBrasseur, M. T. Drake, R. J. Pignolo, T. Pirtskhalava, T. Tchkonia, M. J. Oursler, J. L. Kirkland, S. Khosla, Targeting cellular senescence prevents age-related bone loss in mice. *Nat. Med.* **23**, 1072–1079 (2017).
117. L. J. Hickson, L. G. P. Langhi Prata, S. A. Bobart, T. K. Evans, N. Giorgadze, S. K. Hashmi, S. M. Herrmann, M. D. Jensen, Q. Jia, K. L. Jordan, T. A. Kellogg, S. Khosla, D. M. Koerber, A. B. Lagnado, D. K. Lawson, N. K. LeBrasseur, L. O. Lerman, K. M. McDonald, T. J. McKenzie, J. F. Passos, R. J. Pignolo, T. Pirtskhalava, I. M. Saadiq, K. K. Schaefer, S. C. Textor, S. G. Victorelli, T. L. Volkman, A. Xue, M. A. Wentworth, E. O. Wissler Gerdes, Y. Zhu, T. Tchkonia, J. L. Kirkland, Senolytics decrease senescent cells in humans: Preliminary report from a clinical trial of Dasatinib plus Quercetin in individuals with diabetic kidney disease. *EBioMedicine* **47**, 446–456 (2019).
118. M. J. Schafer, T. A. White, K. Iijima, A. J. Haak, G. Ligresti, E. J. Atkinson, A. L. Oberg, J. Birch, H. Salmonowicz, Y. Zhu, D. L. Mazula, R. W. Brooks, H. Fuhrmann-Stroissnigg, T. Pirtskhalava, Y. S. Prakash, T. Tchkonia, P. D. Robbins, M. C. Aubry, J. F. Passos, J. L. Kirkland, D. J. Tschumperlin, H. Kita, N. K. LeBrasseur, Cellular senescence mediates fibrotic pulmonary disease. *Nat. Commun.* **8**, 14532 (2017).
119. P. R. Coryell, B. O. Diekman, R. F. Loeser, Mechanisms and therapeutic implications of cellular senescence in osteoarthritis. *Nat. Rev. Rheumatol.* **17**, 47–57 (2021).
120. O. H. Jeon, N. David, J. Campisi, J. H. Elisseeff, Senescent cells and osteoarthritis: A painful connection. *J. Clin. Invest.* **128**, 1229–1237 (2018).
121. S. K. Dehkordi, J. Walker, E. Sah, E. Bennett, F. Atrian, B. Frost, B. Woost, R. E. Bennett, T. C. Orr, Y. Zhou, P. S. Andhey, M. Colonna, P. H. Sudmant, P. Xu, M. Wang, B. Zhang, H. Zare, M. E. Orr, Profiling senescent cells in human brains reveals neurons with CDKN2D/p19 and tau neuropathology. *Nat. Aging.* **1**, 1107–1116 (2021).
122. V. Borgonetti, N. Galeotti, Microglia senescence is related to neuropathic pain-associated comorbidities in the spared nerve injury model. *Pain* **164**, 1106–1117 (2023).
123. S. J. Chinta, G. Woods, M. Demaria, A. Rane, Y. Zou, A. McQuade, S. Rajagopalan, C. Limbad, D. T. Madden, J. Campisi, J. K. Andersen, Cellular senescence is induced by the environmental neurotoxin paraquat and contributes to neuropathology linked to Parkinson's Disease. *Cell Rep.* **22**, 930–940 (2018).
124. S. Gaikwad, N. Puangmalai, A. Bittar, M. Montalbano, S. Garcia, S. McAllen, N. Bhatt, M. Sonawane, U. Sengupta, R. Kayed, Tau oligomer induced HMGB1 release contributes to cellular senescence and neuropathology linked to Alzheimer's disease and frontotemporal dementia. *Cell Rep.* **36**, 109419 (2021).
125. R. Bhat, E. P. Crowe, A. Bitto, M. Moh, C. D. Katsetos, F. U. Garcia, F. B. Johnson, J. Q. Trojanowski, C. Sell, C. Torres, Astrocyte senescence as a component of Alzheimer's disease. *PLOS ONE* **7**, e45069 (2012).
126. J. Cohen, C. Torres, Astrocyte senescence: Evidence and significance. *Aging Cell* **18**, e12937 (2019).
127. J. Du, N. Cheng, Y. Deng, P. Xiang, J. Liang, Z. Zhang, Z. Hei, X. Li, Astrocyte senescence-like response related to peripheral nerve injury-induced neuropathic pain. *Cell. Mol. Biol. Lett.* **28**, 65 (2023).
128. S. Lin, C. Xu, X. Yin, H. Tian, X. Mei, Aging and TNF induce premature senescence of astrocytes after spinal cord injury via regulating YAP expression. *Int. Immunopharmacol.* **120**, 110276 (2023).
129. K. Simmnacher, F. Krach, Y. Schneider, J. E. Alecu, L. Mautner, P. Klein, L. Roybon, I. Prots, W. Xiang, B. Winner, Unique signatures of stress-induced senescent human astrocytes. *Exp. Neurol.* **334**, 113466 (2020).
130. T. Matsudaira, S. Nakano, Y. Konishi, S. Kawamoto, K. Uemura, T. Kondo, K. Sakurai, T. Ozawa, T. Hikida, O. Komine, K. Yamanaka, Y. Fujita, T. Yamashita, T. Matsumoto, E. Hara, Cellular senescence in white matter microglia is induced during ageing in mice and exacerbates the neuroinflammatory phenotype. *Commun. Biol.* **6**, 665 (2023).
131. A. Muralidharan, S. G. Sotocinal, N. Yousefpour, N. Akkurt, L. V. Lima, S. Tansley, M. Parisien, C. Wang, J.-S. Austin, B. Ham, G. M. Dutra, P. Rousseau, S. Maldonado-Bouchard, T. Clark, S. F. Rosen, M. R. Majeed, O. Silva, R. Nejade, X. Li, S. D. Pimentel, C. S. Nielsen, G. G. Neely, C. Autexier, L. Diatchenko, A. Ribeiro-da-Silva,

J. S. Mogil, Long-term male-specific chronic pain via telomere- and p53-mediated spinal cord cellular senescence. *J. Clin. Invest.* **132**, e151817 (2022).
132. Y. Kawasaki, Z. Z. Xu, X. Wang, J. Y. Park, Z. Y. Zhuang, P. H. Tan, Y. J. Gao, K. Roy, G. Corfas, E. H. Lo, R. R. Ji, Distinct roles of matrix metalloproteases in the early- and late-phase development of neuropathic pain. *Nat. Med.* **14**, 331–336 (2008).
133. S. B. McMahon, M. Malcangio, Current challenges in glia-pain biology. *Neuron* **64**, 46–54 (2009).
134. C. Lopez-Otin, M. A. Blasco, L. Partridge, M. Serrano, G. Kroemer, The hallmarks of aging. *Cell* **153**, 1194–1217 (2013).
135. J. R. Herdy, J. Mertens, F. H. Gage, Neuronal senescence may drive brain aging. *Science* **384**, 1404–1406 (2024).
136. D. J. Baker, R. C. Petersen, Cellular senescence in brain aging and neurodegenerative diseases: Evidence and perspectives. *J. Clin. Invest.* **128**, 1208–1216 (2018).
137. A. Salminen, J. Ojala, K. Kaarniranta, A. Haapasalo, M. Hiltunen, H. Soininen, Astrocytes in the aging brain express characteristics of senescence-associated secretory phenotype. *Eur. J. Neurosci.* **34**, 3–11 (2011).
138. R. J. Evans, F. S. Wyllie, D. Wynford-Thomas, D. Kipling, C. J. Jones, A P53-dependent, telomere-independent proliferative life span barrier in human astrocytes consistent with the molecular genetics of glioma development. *Cancer Res.* **63**, 4854–4861 (2003).
139. A. Bitto, C. Sell, E. Crowe, A. Lorenzini, M. Malaguti, S. Hrelia, C. Torres, Stress-induced senescence in human and rodent astrocytes. *Exp. Cell Res.* **316**, 2961–2968 (2010).
140. J. Hou, C. Cui, S. Kim, C. Sung, C. Choi, Ginsenoside F1 suppresses astrocytic senescence-associated secretory phenotype. *Chem. Biol. Interact.* **283**, 75–83 (2018).
141. C. Rim, M. J. You, M. Nahm, M. S. Kwon, Emerging role of senescent microglia in brain aging-related neurodegenerative diseases. *Transl Neurodegener.* **13**, 10 (2024).
142. H. M. Yu, Y. M. Zhao, X. G. Luo, Y. Feng, Y. Ren, H. Shang, Z. Y. He, X. M. Luo, S. D. Chen, X. Y. Wang, Repeated lipopolysaccharide stimulation induces cellular senescence in BV2 cells. *Neuroimmunomodulation* **19**, 131–136 (2012).
143. W. J. Streit, H. Braak, Q. S. Xue, I. Bechmann, Dystrophic (senescent) rather than activated microglial cells are associated with tau pathology and likely precede neurodegeneration in Alzheimer's disease. *Acta Neuropathol.* **118**, 475–485 (2009).
144. B. E. Flanary, N. W. Sammons, C. Nguyen, D. Walker, W. J. Streit, Evidence that aging and amyloid promote microglial cell senescence. *Rejuvenation Res.* **10**, 61–74 (2007).
145. Y. Kujuro, N. Suzuki, T. Kondo, Esophageal cancer-related gene 4 is a secreted inducer of cell senescence expressed by aged CNS precursor cells. *Proc. Natl. Acad. Sci. U.S.A.* **107**, 8259–8264 (2010).
146. D. Jurk, C. Wang, S. Miwa, M. Maddick, V. Korolchuk, A. Tsolou, E. S. Gonos, C. Thrasivoulou, M. J. Saffrey, K. Cameron, T. von Zglinicki, Postmitotic neurons develop a p21-dependent senescence-like phenotype driven by a DNA damage response. *Aging Cell* **11**, 996–1004 (2012).
147. N. He, W. L. Jin, K. H. Lok, Y. Wang, M. Yin, Z. J. Wang, Amyloid-β_{1-42} oligomer accelerates senescence in adult hippocampal neural stem/progenitor cells via formylpeptide receptor 2. *Cell Death Dis.* **4**, e924 (2013).
148. W. Q. Li, Z. J. Wang, S. Liu, Y. Hu, M. Yin, Y. Lu, N-Stearoyl-L-tyrosine inhibits the senescence of neural stem/progenitor cells induced by Aβ_{1-42} via the CB2 receptor. *Stem Cells Int.* **2016**, 7419389 (2016).
149. R. Bose, M. Moors, R. Tofighi, A. Cascante, O. Hermanson, S. Ceccatelli, Glucocorticoids induce long-lasting effects in neural stem cells resulting in senescence-related alterations. *Cell Death Dis.* **1**, e92 (2010).
150. Y. Wang, K. Kuca, L. You, E. Nepovimova, Z. Heger, M. Valko, V. Adam, Q. Wu, K. Jomova, The role of cellular senescence in neurodegenerative diseases. *Arch. Toxicol.* **98**, 2393–2408 (2024).
151. D. Paramos-de-Carvalho, A. Jacinto, L. Saude, The right time for senescence. *eLife* **10**, e72449 (2021).
152. K. Yamakoshi, A. Takahashi, F. Hirota, R. Nakayama, N. Ishimaru, Y. Kubo, D. J. Mann, M. Ohmura, A. Hirao, H. Saya, S. Arase, Y. Hayashi, K. Nakao, M. Matsumoto, N. Ohtani, E. Hara, Real-time in vivo imaging of p16Ink4a reveals cross talk with p53. *J. Cell Biol.* **186**, 393–407 (2009).
153. H.-N. Kim, J. Xiong, R. S. MacLeod, S. Iyer, Y. Fujiwara, K. M. Cawley, L. Han, Y. He, J. D. Thostenson, E. Ferreira, R. L. Jilka, D. Zhou, M. Almeida, C. A. O'Brien, Osteocyte RANKL is required for cortical bone loss with age and is induced by senescence. *JCI Insight* **5**, e138815 (2020).
154. R. J. Pignolo, J. F. Passos, S. Khosla, T. Tchkonia, J. L. Kirkland, Reducing senescent cell burden in aging and disease. *Trends Mol. Med.* **26**, 630–638 (2020).
155. A. K. Sharma, R. L. Roberts, R. D. Benson Jr., J. L. Pierce, K. Yu, M. W. Hamrick, M. E. McGee-Lawrence, The senolytic drug navitoclax (ABT-263) causes trabecular bone loss and impaired osteoprogenitor function in aged mice. *Front. Cell Dev. Biol.* **8**, 354 (2020).
156. M. Mantzorou, E. Pavlidou, G. Vasios, E. Tsagalioti, C. Giaginis, Effects of curcumin consumption on human chronic diseases: A narrative review of the most recent clinical data. *Phytother. Res.* **32**, 957–975 (2018).
157. A. S. Oliveira, E. Sousa, M. H. Vasconcelos, M. Pinto, Curcumin: A natural lead for potential new drug candidates. *Curr. Med. Chem.* **22**, 4196–4232 (2015).
158. Y. J. Moon, L. Wang, R. DiCenzo, M. E. Morris, Quercetin pharmacokinetics in humans. *Biopharm. Drug Dispos.* **29**, 205–217 (2008).
159. Y. C. Hou, P. D. Chao, H. J. Ho, C. C. Wen, S. L. Hsiu, Profound difference in pharmacokinetics between morin and its isomer quercetin in rats. *J. Pharm. Pharmacol.* **55**, 199–203 (2003).
160. L. L. Yang, N. Xiao, X. W. Li, Y. Fan, R. N. Alolga, X. Y. Sun, S. L. Wang, P. Li, L. W. Qi, Pharmacokinetic comparison between quercetin and quercetin 3-*O*-β-glucuronide in rats by UHPLC-MS/MS. *Sci. Rep.* **6**, 35460 (2016).
161. D. Leveque, G. Becker, K. Bilger, S. Natarajan-Ame, Clinical pharmacokinetics and pharmacodynamics of dasatinib. *Clin. Pharmacokinet.* **59**, 849–856 (2020).
162. W. B. Hassouneh, M. A. Al-Ghazawi, M. I. Saleh, N. Najib, Population pharmacokinetics of dasatinib in healthy subjects. *Pharmaceuticals* **17**, 671 (2024).
163. A. B. Nair, S. Jacob, A simple practice guide for dose conversion between animals and human. *J. Basic Clin. Pharmacol.* **7**, 27–31 (2016).
164. M. M. Gonzales, V. R. Garbarino, E. Marques Zilli, R. C. Petersen, J. L. Kirkland, T. Tchkonia, N. Musi, S. Seshadri, S. Craft, M. E. Orr, Senolytic therapy to modulate the progression of Alzheimer's disease (SToMP-AD): A pilot clinical trial. *J. Prev Alzheimers Dis.* **9**, 22–29 (2022).
165. Y. Zhu, L. Prata, E. O. W. Gerdes, J. M. E. Netto, T. Pirtskhalava, N. Giorgadze, U. Tripathi, C. L. Inman, K. O. Johnson, A. Xue, A. K. Palmer, T. Chen, K. Schaefer, J. N. Justice, A. M. Nambiar, N. Musi, S. B. Kritchevsky, J. Chen, S. Khosla, D. Jurk, M. J. Schafer, T. Tchkonia, J. L. Kirkland, Orally-active, clinically-translatable senolytics restore α-Klotho in mice and humans. *EBioMedicine* **77**, 103912 (2022).
166. A. Nambiar, D. Kellogg III, J. Justice, M. Goros, J. Gelfond, R. Pascual, S. Hashmi, M. Masternak, L. Prata, N. LeBrasseur, A. Limper, S. Kritchevsky, N. Musi, T. Tchkonia, J. Kirkland, Senolytics dasatinib and quercetin in idiopathic pulmonary fibrosis: Results of a phase I, single-blind, single-center, randomized, placebo-controlled pilot trial on feasibility and tolerability. *EBioMedicine* **90**, 104481 (2023).
167. J. N. Justice, A. M. Nambiar, T. Tchkonia, N. K. LeBrasseur, R. Pascual, S. K. Hashmi, L. Prata, M. M. Masternak, S. B. Kritchevsky, N. Musi, J. L. Kirkland, Senolytics in idiopathic pulmonary fibrosis: Results from a first-in-human, open-label, pilot study. *EBioMedicine* **40**, 554–563 (2019).
168. M. Alini, S. M. Eisenstein, K. Ito, C. Little, A. A. Kettler, K. Masuda, J. Melrose, J. Ralphs, I. Stokes, H. J. Wilke, Are animal models useful for studying human disc disorders/degeneration? *Eur. Spine J.* **17**, 2–19 (2008).
169. K. Norose, J. I. Clark, N. A. Syed, A. Basu, E. Heber-Katz, E. H. Sage, C. C. Howe, SPARC deficiency leads to early-onset cataractogenesis. *Invest. Ophthalmol. Vis. Sci. 39*, 2674–2680 (1998).
170. M. Tajerian, M. Millecamps, L. S. Stone, Morphine and clonidine synergize to ameliorate low back pain in mice. *Pain Res. Treat.* **2012**, 150842 (2012).
171. S. Lee, M. Millecamps, D. Z. Foster, L. S. Stone, Long-term histological analysis of innervation and macrophage infiltration in a mouse model of intervertebral disc injury-induced low back pain. *J. Orthop. Res.* **38**, 1238–1247 (2020).
172. J. R. Deuis, L. S. Dvorakova, I. Vetter, Methods used to evaluate pain behaviors in rodents. *Front. Mol. Neurosci.* **10**, 284 (2017).
173. S. R. Chaplan, F. W. Bach, J. W. Pogrel, J. M. Chung, T. L. Yaksh, Quantitative assessment of tactile allodynia in the rat paw. *J. Neurosci. Methods* **53**, 55–63 (1994).
174. V. Y. L. Leung, W. C. W. Chan, S.-C. Hung, K. M. C. Cheung, D. Chan, Matrix Remodeling During Intervertebral Disc Growth and Degeneration Detected by Multichromatic FAST Staining. *J. Histochem. Cytochem.* **57**, 249–256 (2008); https://doi.org/10.1369/jhc.2008.952184.
175. C. Gao, B. P. Chen, M. B. Sullivan, J. Hui, J. A. Ouellet, J. E. Henderson, N. Saran, Micro CT analysis of spine architecture in a mouse model of scoliosis. *Front. Endocrinol.* **6**, 38 (2015).

Acknowledgments: We thank the staff of McGill University's ABC-platform (Animal Behavioral Characterization) at the Alan Edwards Centre for Research on Pain and Animal Resources Center. **Funding:** This work was supported by the CIHR, grants PJT-178111, MOP-142291 (to L.S., L.H., J.A.O., and M.Mi.), and PJT-173355 (to R.S.N.); Arthritis Society, grant SOG-20-0000000075 (to L.H., L.S.S., M.Mi., and J.A.O.); and a major infrastructure grant from Le Réseau de Recherche en Santé Buccodentaire et Osseuse (RSBO) (to L.H.). Doctoral training awards: CIHR, no. 476767 (to M.Ma.); Arthritis Society, TGP-20-0000000063 (to M.Ma.) and TGP-23-0000000210 (to S.G.); Louise and Alan Edwards Foundation's studentship in Pain Research, no. 2073 (to M.Ma.); and Le Réseau de Recherche en Santé Buccodentaire et Osseuse (RSBO), 20-0000000063 (to M.Ma.). Postdoctoral award: Arthritis Society, TPF-19-0513 (to H.C.). **Author contributions:** Conceptualization: L.H., L.S.S., J.A.O., and H.C. Methodology: L.H., L.S.S., J.A.O., H.C., and M.Mi. Investigation: M.Ma., H.C., S.G., O.W.M., K.S., E.C., and S.L. Visualization: M.Ma., H.C., S.G., O.W.M., K.S., E.C., and S.L. Supervision: L.H., L.S.S., H.C., M.Mi. Writing—original draft: L.H. and H.C.

Writing—review and editing: L.H., H.C., M.Ma., L.S.S., J.A.O., M.Mi., S.G., O.W.M., K.S., E.C., S.L., C.G., R.S.N., C.P., and A.G. **Competing interests:** The authors declare that they have no competing interests. **Data and materials availability:** All data needed to evaluate the conclusions in the paper are present in the paper and/or the Supplementary Materials.

Submitted 19 June 2024
Accepted 7 February 2025
Published 14 March 2025
10.1126/sciadv.adr1719